Highly replicated evolution of parapatric ecotypes

Maddie E. James[1], Henry Arenas-Castro[1], Jeffrey S. Groh[1,2], Scott L. Allen[1], Jan Engelstädter[1], Daniel Ortiz-Barrientos[1]

[1]The University of Queensland, School of Biological Sciences, St. Lucia QLD 4072, Australia. [2]Current address: University of California, Davis, Center for Population Biology and Department of Evolution and Ecology, Davis, CA 95616, United States.

Corresponding author: Maddie E. James; maddie.james@uqconnect.edu.au

Abstract

Parallel evolution of ecotypes occurs when selection independently drives the evolution of similar traits across similar environments. The multiple origin of ecotypes is often inferred on the basis of a phylogeny which clusters populations according to geographic location and not by the environment they occupy. However, the use of phylogenies to infer parallel evolution in closely related populations is problematic because gene flow and incomplete lineage sorting can uncouple the genetic structure at neutral markers from the colonization history of populations. Here, we demonstrate multiple origins within ecotypes of an Australian wildflower, *Senecio lautus*. We observed strong genetic structure as well as phylogenetic clustering by geography and show that this is unlikely due to gene flow between parapatric ecotypes, which is surprisingly low. We further confirm this analytically by demonstrating that phylogenetic distortion due to gene flow often requires higher levels of migration than those observed in *S. lautus*. Our results imply that selection can repeatedly create similar phenotypes despite the perceived homogenizing effects of gene flow.

Introduction

Parallel evolution occurs when populations evolve similar traits after repeatedly and independently colonizing similar habitats (Schluter and Nagel 1995). When the distribution of habitats is patchy, phenotypically similar populations frequently occur next to other contrasting phenotypes (e.g., plant species adapted to serpentine and non-serpentine soils in Scandinavia; Berglund et al. 2003, and marine snails adapted to crab predators or wave action along the rocky coasts of Europe; Johannesson et al. 2010). Parallel evolution by natural selection creates consistent patterns of phenotypic similarity and divergence that can extend to morphological (Elmer et al. 2010; Ravinet et al. 2013; Perreault-Payette et al. 2017), behavioral (York and Fernald 2017), and reproductive (Smith and Rausher 2011) traits, yet there is often variation in the extent to which replicate populations exhibit similar phenotypes (see Bolnick et al. 2018). The nature of parallel trait evolution largely depends on the demographic history of the system under investigation, where the interplay of geography, gene flow, and natural selection along with the genetic architecture of traits determines its repeatability (Orr 2005; Stern and Orgogozo 2009; Rosenblum et al. 2014; Lenormand et al. 2016; Stoltzfus and McCandlish 2017; Blount et al. 2018; Yeaman et al. 2018). However, it is surprisingly rare for studies of parallel evolution to convincingly demonstrate that

populations exhibiting similar phenotypes have arisen in an independent and repeated fashion ('multiple origin' scenario). Ruling out alternative demographic scenarios, such as a single origin of ecotypes followed by gene flow upon secondary contact, is seldom performed (but see work in *Littorina* and stickleback, Quesada et al. 2007; Bierne et al. 2013; Butlin et al. 2014; Pérez-Pereira et al. 2017, and see Ostevik et al. 2012 for a critical review of the evidence in plants). In light of this, researchers may incorrectly assume a parallel demographic history, leading to inaccurate inferences about the prevalence of parallel evolution in nature.

Typically, researchers identify parallel evolution by natural selection by asking whether phylogenetic clustering of populations (estimated in the absence of gene flow) coincides with the geographic distribution of populations (geography) and not with the habitat in which they occur (ecology) (Allender et al. 2003; Quesada et al. 2007; Johannesson et al. 2010; Butlin et al. 2014; Trucchi et al. 2017). This is because genetic clustering of geographically close populations implies dispersal might be geographically restricted (i.e., isolation by distance; Wright 1943), and colonization of contrasting and neighboring habitats might have occurred independently many times. The rationale for this argument is that the genome-wide phylogenetic history across the geographic range of populations can reveal the history of adaptation. That is, if the repeated evolution of similar phenotypes appears to have taken place on different genetic backgrounds (lineages), then the genetic changes that drove adaptation likely occurred independently. By genetic changes, we refer specifically to independent allele frequency changes driven by similar natural selection pressures.

The above argument rests upon the assumption that the genome-wide pattern of relatedness accurately depicts the history of the loci underlying adaptation, although this is not necessarily the case. For example, alternative historical scenarios could also lead to clustering of populations by geography, and must be ruled out before examining the evolution of traits in light of parallel evolution (Endler 1977; Barton and Hewitt 1985; Coyne and Orr 2004; Bierne et al. 2013). For instance, a recent phylogenomic analysis of *Mimulus* section *Erythranthe* overturned a classical example of putative convergence in hummingbird pollination (Beardsley et al. 2004; Freeman and Herron 2004). The authors discovered that hummingbird pollination in the genus arose only once, yet over a large portion of the genome, sympatric populations of *M. cardinalis* (hummingbird-pollinated) and *M. lewisii* (bee-pollinated) appear as sister taxa in the phylogeny because of multiple introgression

events after periods of allopatry (Nelson et al. 2021). To understand how demography, geography and selection contribute to our interpretations of parallel evolution, first consider a scenario where an ancestral population gives rise to two locally adapted populations that occupy ecologically distinct yet geographically proximate habitats (hereafter ecotypes, Fig. 1A). These two populations repeatedly migrate to new localities, where each time the same contrasting habitats are geographically close. This scenario of a single split followed by range expansion of two ecotypes does not involve a parallel adaptation history because each ecotype only arose once (rather than multiple independent times after independent colonization of contrasting habitats). Because gene flow is either not possible after the original ecotypic split due to complete reproductive isolation, or gene flow does not homogenize adjacent populations after range expansion, populations sharing the same ecology form reciprocally monophyletic clades in a phylogeny (Fig. 1A, *Single origin without gene flow*).

Nevertheless, if there is sufficient gene flow between geographically close populations from two ecotypes that originated only once (like the *Mimulus* example described above), the original phylogenetic signal of reciprocal monophyly could be eroded (Endler 1977; Barton and Hewitt 1985; Coyne and Orr 2004; Bierne et al. 2013). In other words, as the original genome-wide phylogenetic signal of a single origin disappears, populations become most related to their neighboring population and not to the other populations of the same ecotype. Therefore, gene flow can result in grouping of populations by geography rather than ecology (Fig. 1B, *Single origin with gene flow*). This phylogenetic signal is identical to that of true parallel evolution (a multiple origin scenario), where the derived ecotype arises multiple independent times from the ancestral ecotype (Fig. 1C, *Multiple origins*). Gene flow dynamics can thus fundamentally alter our interpretation of parallel evolution, to the extent that we can mistakenly infer parallel evolution in systems where secondary contact after range expansion of a single origin has obscured the history of locally adapted populations (Endler 1977; Barton and Hewitt 1985; Coyne and Orr 2004; Bierne et al. 2013).

Despite the potential for gene flow to paint a false picture of the phylogenetic history of multiple populations adapted to the same environment, it is important to note that non-monophyly of populations from the same ecotype is not a requirement for parallel evolution in a more general sense. This is because it is possible that two populations of the same ecotype that are true phylogenetic sister groups did in fact adapt independently. However,

103 non-monophyly of each ecotype is a requirement in systems where parallel evolution
104 coincides with a patchy geographic distribution of populations (pairs of ecotypes in multiple
105 localities; Bierne et al. 2013), where the phylogenetic line of reasoning is commonly
106 employed.

107 In systems of parallel evolution, gene flow is frequently detected between populations,
108 especially when contrasting ecotypes are in close geographic proximity (i.e., parapatry).
109 Although not all levels of gene flow have the same effect on the genetic record of
110 colonization history (Bierne et al. 2013), gene flow between ecotypes must be taken into
111 account when demonstrating parallel origins within a system. However, only very few
112 systems have thoroughly investigated the demographic history of populations, and even
113 fewer have used coalescent modelling or simulations to address whether the estimated levels
114 of gene flow could have obscured the observed phylogeny. A system that has clearly
115 demonstrated the parallel origins of contrasting populations in the presence of gene flow is
116 the marine snail *Littorina saxatilis*. Multiple lines of evidence suggest the wave and crab
117 ecotypes evolved multiple independent times along rocky coastlines (Quesada et al. 2007;
118 Johannesson et al. 2010; Bierne et al. 2013; Butlin et al. 2014; Pérez-Pereira et al. 2017).
119 Other systems providing evidence for parallel evolution include Lake Victoria cichlids
120 (Meier et al. 2017) and alpine and montane *Heliosperma pusillum* ecotypes (Trucchi et al.
121 2017). Also, an obvious case showing multiple origins is when parallel evolution occurs
122 between geographically distant populations where gene flow could not have obscured the
123 phylogenetic signal and demographic history of populations (e.g., threespine stickleback
124 populations that colonized freshwater environments on separate continents; Magalhaes et al.
125 2020). However, in other systems, where gene flow is moderate between ecotypes
126 (Rougemont et al. 2015; Le Moan et al. 2016; Rougeux et al. 2017; Herman et al. 2018;
127 Rougeux et al. 2019), it remains unclear to what extent gene flow contributed to the signal of
128 parallel evolution.

129 We must keep in mind that identifying the genetic basis of parallel trait evolution often
130 provides unambiguous evidence for parallel evolution of ecotypes. For instance, in
131 sticklebacks, the repeated evolution of the reduction of pelvic armor in separate populations
132 occurred via different mutations in the same gene (Chan et al. 2010), suggesting this adaptive
133 trait has arisen and been selected for multiple independent times. In contrast, in systems
134 where the exact same mutation is repeatedly involved in adaptation (e.g., Colosimo et al.

135 2005), it is challenging to identify whether the adaptive mutation was repeatedly and
136 independently selected for in each population (either from de-novo mutations or via standing
137 genetic variation; Roesti et al. 2014; Lee and Coop 2019). Knowing the causal genes of
138 adaptation is ideal as the demographic history of individual adaptive loci can be modelled,
139 avoiding the complications of distinguishing between single and multiple origins using
140 neutral polymorphisms (as described above). However, directly isolating the specific genes
141 involved in adaptation is infeasible in most non-model organisms or when the genetic
142 architecture of adaptation is highly polygenic (Tiffin and Ross-Ibarra 2014; Yeaman 2015).

143 The above considerations suggest that without knowing the genetic basis of parallel
144 adaptation, we should carefully characterize and interpret the phylogeographic history to
145 understand the level of independence in systems where populations are adapted to similar
146 environments. Such an approach is necessary to demonstrate that natural selection has
147 independently acted in separate populations during the repeated adaptation to similar
148 environments. This knowledge paves the way for future research on dissecting the molecular
149 basis of parallel adaptation, and has implications for our understanding of how repeatable and
150 predictable evolution can be. In this work, we thoroughly characterize the phylogenetic and
151 demographic history of *Senecio lautus*, an Australian wildflower that appears to have evolved
152 multiple times in parapatry into two contrasting coastal forms called Dune and Headland
153 ecotypes (Roda, Ambrose, et al. 2013; Melo et al. 2014). The two forms differ in their growth
154 habit: the Dune ecotype is erect and inhabits sand dunes, and the Headland ecotype is
155 prostrate, forming matts on the ground of rocky headlands (Ali 1964; Radford et al. 2004;
156 Thompson 2005). These locally adapted populations (Melo et al. 2014; Richards et al. 2016;
157 Richards and Ortiz-Barrientos 2016; Walter et al. 2016; Walter, Wilkinson, et al. 2018;
158 Wilkinson et al. 2021) are separated by strong extrinsic reproductive isolation (Melo et al.
159 2014; Richards et al. 2016), and populations exhibit similar morphology within each ecotype
160 (Walter, Aguirre, et al. 2018; James et al. 2020). With this work we hope to clearly illustrate
161 how the demographic history of populations affects the evidence for the independent and
162 repeated origins of parapatric ecotypes.

163 Previous work using pools of DNA sequences from multiple coastal, inland, alpine, and
164 woodland *S. lautus* ecotypes found that strong isolation by distance separated all populations
165 along the coast and that geography, not ecology, explained the phylogenetic clustering of
166 coastal populations (Roda, Ambrose, et al. 2013). Although these results initially suggested

that the Dune and Headland ecotypes evolved in parallel, it remains unclear if gene flow could be responsible for this pattern of ecotypic and geographic differentiation. Therefore, our inferences on the number of independent colonization and origin events of Dune and Headland populations remains unclear. Here, we directly estimate patterns of gene flow between 23 Dune and Headland populations, as well as other parameters important for characterizing the demographic history of this system. We create a coalescent model and undertake simulations to explore the conditions that could erode a signal of phylogenetic monophyly of each ecotype, thus enabling us to gain further confidence in our conclusions about parallel parapatric divergence in this system. Our results enhance our understanding of the nature of parallel evolution and pave the way for analyses of parallel trait evolution driven by natural selection in plants, where cases of parallelism remain understudied.

Results

Populations cluster by geography and not by ecology

To ask whether populations cluster according to their geographic distribution, we explored broad patterns of genetic clustering across the 23 Dune and Headland *S. lautus* populations (Fig. 2A). Phylogenetic inference in *IQ-TREE* provides evidence against a single origin scenario: neither ecotype forms a monophyletic clade, and parapatric Dune-Headland populations are often sister-taxa, consistent with a possible multiple origin of ecotypes (Fig. 2B). To visualize the major genetic structure within *fastSTRUCTURE*, we plotted the lowest K-values that capture the major structure in the data as suggested by Pritchard et al. (2000) and Lawson et al. (2018), although the "best" K-value across all populations was higher (see below). The clustering of populations into two genetic groups (K=2) revealed a striking correspondence to geography (Fig. 2C), where the eastern populations (dark blue) are separated from those populations further south and to the west (light blue). This division into two main clades probably suggests some past geographic separation. When three genetic groups (K=3) are considered, the eastern populations are further separated into two clusters, again largely corresponding to geography and reflecting the phylogenetic structure of the data; K=4 distinguishes the west Australia populations from those on the south-eastern coast.

195 **Minimal admixture across the system**

196 To understand the role of gene flow in shaping the patterns of divergence across the system,
197 we explored patterns of admixture in a phylogenetic context within *TreeMix*. In the absence
198 of migration, the *TreeMix* phylogeny explained 95.9% of the data, with 24 additional
199 migration events augmenting this value to 98.9 % (Supplementary Fig. S1). Fig. 3A shows
200 the first migration event ($P < 2.2x10^{-308}$) with a migration weight (*w*) of 0.40. Although the
201 24 other migration events were also significant ($P_{average} = 2.92x10^{-3}$, SD = 0.0062), their
202 individual weightings were small (see Supplementary Fig. S2 for 1-10 migration events),
203 most of them were not between parapatric pairs, and the addition of these migration events
204 did not substantially alter the topology from its estimation in the absence of gene flow.
205 Although these results could suggest a potentially complex colonization history including
206 long distance yet rare migration events, these P-values should be treated with caution. This is
207 because model comparisons in *TreeMix* suffer from multiple testing, a large number of
208 parameters, and the estimated graph can be inaccurate (Pickrell and Pritchard 2012). We
209 therefore tested the robustness of this inference using *f3-statistics*. All *f3-statistics* were
210 positive (Supplementary Fig. S3), giving no evidence of admixture between any populations.
211 Strong isolation by distance within each ecotype further supports this contention using $\widehat{M}$ as a
212 proxy for migration rates (IBD within Dunes: Mantel test, r = -0.83, P = 0.0001; within
213 Headlands r = -0.73, P = <0.0001; Fig. 3B). A strong IBD trend also exists between ecotypes
214 for the eight pairs studied here ($\widehat{M}$: $F_{1,6} = 0.55$, P = 0.05661, multiple $R^2 = 0.48$, Fig. 3B).
215 Although the same trend was seen in the migration rate estimates from *fastsimcoal2*, it was
216 not statistically significant, perhaps due to the low sample size (*fastsimcoal2*: $F_{1,6} = 0.66$, P =
217 0.4475, multiple $R^2 = 0.10$, Fig. 3C).

218 The absence of admixture across the system is also supported by *fastSTRUCTURE* across all
219 populations. The inferred value of K is close to the number of sampled populations
220 (Supplementary Figs. S4B, S4C) and each population is genetically distinct (Supplementary
221 Fig. S4A), suggesting that *S. lautus* has a simple demographic history with limited admixture
222 (Lawson et al. 2018). Specifically, the K-value that best explained the structure in the data
223 was 22, and the K-value that maximized the marginal likelihood of the data was 28
224 (Supplementary Fig. S4B). The rate of change in the likelihood of each K-value was
225 negligible for K=24-28 (Supplementary Fig. S4C). Together, this suggests that the optimal
226 K-value is around 23, which is the number of populations within our study. The

227 *fastSTRUCTURE* results for K=23 show that each population forms a distinct genetic cluster
228 (Fig. 3D), suggesting very little, if any, admixture between them. This further implies that
229 each sampled population has been separated from other populations long enough to be
230 genetically distinct (see pairwise F_{ST} values in Supplementary Table S1), and with
231 insufficient levels of gene flow to homogenize their genomes (Lawson et al. 2018). Further,
232 when we examined all K-values from 1-23, we found a distinct hierarchical structure that
233 mirrors the phylogeny, suggesting that such structure is an accurate representation of the
234 history of the populations. The Tasmania population pair (D14-H15) should be treated with
235 caution due to the smaller sample size (n_{Dune} = 12, $n_{Headland}$ = 11) compared to other
236 populations (n_{mean} = 62, SD = 1.19). For groups with few samples, genetic clustering
237 programs such as *fastSTRUCTURE* are likely to assign them as mixtures of multiple
238 populations rather than their own distinct population (Lawson et al. 2018). This is evident for
239 K=22, where the Tasmania populations appear admixed (Supplementary Fig. S4A).

240 **Minimal gene flow between parapatric ecotypes and distant populations**

241 We investigated whether the parapatric ecotypes at each locality have diverged in the face of
242 gene flow by analyzing patterns of admixture in *STRUCTURE* and directly estimating levels
243 of gene flow in *fastsimcoal2.* We observed very few admixed individuals between the
244 parapatric Dune-Headland populations at each locality within the *STRUCTURE* analysis for
245 K=2 (Fig. 4A). On average, 9.36% (SD = 5.48) of individuals were admixed per population,
246 although their admixture proportions were on average less than 1% (mean = 0.8%, SD = 1.8).
247 This suggests that gene flow between parapatric populations might be rare and ongoing, or
248 might have ceased in the past. For all pairs, the best K-value based on the Evanno method
249 (Evanno et al. 2005) was K=2 (Supplementary Fig. S5). Demographic modelling in
250 *fastsimcoal2* (Fig. 4B) revealed the most likely divergence model for all but three
251 comparisons within and between ecotypes was bidirectional gene flow after secondary
252 contact (mean w_i = 0.99, SD = 0.05; Supplementary Table S4; Supplementary Fig. S6). For
253 comparisons D04-H05, D14-H15 and D04-D05, the most likely divergence model was
254 ancient bidirectional secondary contact (w_i = 1.00).

255 For Dune-Headland population pairs, direct measurements of migration rates were very low,
256 with all Dune-Headland migration rates below one ($2Nm < 1.00$), except for D04-H05 and
257 D32-H12 where $2Nm$ was above one (Fig. 3C upper section, 4A; Supplementary Tables S2,
258 S3). This is perhaps not surprising given that the populations of D04-H05 are geographically

259 the closest of all parapatric pairs, and the environments of the south-eastern D32-H12
260 populations are less contrasting than populations in the eastern clade. For Dune-Dune
261 comparisons we also detected very low migration rates ($2Nm_{mean}$ = 0.24, SD = 0.09;
262 Supplementary Tables S2, S3), with all comparisons containing $2Nm < 1.00$. Similarly, for
263 Headland-Headland comparisons we again detected very low migration rates ($2Nm_{mean}$ =
264 0.57, SD = 1.08), with all comparisons containing $2Nm < 1.00$, with the exception of H12-
265 H12A (Fig. 3C upper section; Supplementary Tables S2, S3). Across all comparisons, all
266 Dune-Dune pairs and most Headland-Headland pairs exhibited gene flow levels lower than
267 the maximum migration rate of allopatric populations separated by more than 1,500 km (i.e.,
268 the null gene flow expectation; $2Nm = 0.33$; Fig. 3C). Three Dune-Headland pairs (D00-H00,
269 D03-H02 and D12-H14) were also within this null range. Alternative models that assumed
270 very low gene flow, while keeping other demographic parameters fixed, were not a better fit
271 for the data with the exception of the D03-H02 pair (Supplementary Fig. S7). Although the
272 most likely divergence scenario for all population comparisons was bidirectional gene flow
273 after secondary contact and ancient bidirectional secondary contact, migration rates under all
274 models were very low across all population pairs ($2Nm_{mean}$ = 0.68, SD = 1.52, Supplementary
275 Table S4). Thus, even if our choice of model was biased towards secondary contact or
276 models with migration (Roux et al. 2016; Momigliano et al. 2021), the extent of gene flow
277 during the history of populations is consistently low and does not strongly depend upon the
278 mode of divergence.

279 **Potential for gene flow to obscure a single origin scenario**

280 We analyzed a neutral coalescent model representing a single origin of the derived ecotype to
281 investigate under which situations the history at a neutral locus unlinked to the selected site
282 would indicate a pattern of non-monophyly of the derived ecotype, thus potentially
283 supporting a false inference of parallel evolution. We found a clear influence of all examined
284 parameters (Fig. 5A) on the probability of inferring non-monophyly, suggesting that certain
285 demographic scenarios can lead to an observed phylogenetic signal that belies the history of a
286 single origin of ecotypes. When internal branches ($t2 - t1$) are short, incomplete lineage
287 sorting will cause higher probability of non-monophyly, and this is not much increased by
288 migration (Fig. 5B, lower section of graph). When internal branches are long, the probability
289 of non-monophyly is low, and only somewhat more sensitive to increasing migration rate
290 (Fig. 5B, upper section of graph). Long terminal branches ($t1$) also influence the probability

291 of non-monophyly; the more diverged populations contributing migrants are from one
292 another prior to migration into the other ecotype, the more this increases the chances of non-
293 monophyly (Fig. 5C, upper section of graph). This reflects the fact that the introgressed
294 alleles in different recipient populations will have experienced more independent drift prior
295 to the introgression event. When the terminal branches are short relative to the timing of
296 migration, very high levels of migration are required to have a high probability non-
297 monophyly (Fig. 5C, lower section of graph). Note that the probability of non-monophyly is
298 more sensitive to the length of the internal branches, as these determine the likelihood of
299 incomplete lineage sorting (see the different scale of probability in Fig. 5C compared to Fig.
300 5B). Simulation of a single origin scenario with continuous gene flow in *SLiM2* (Haller and
301 Messer 2017) showed patterns consistent with the above coalescent results (Supplementary
302 Fig. S8A).

303 Although we cannot directly map our observed data for *S. lautus* in the modelled or simulated
304 parameter spaces, we can nonetheless explore potential evidence of phylogenetic distortion
305 by examining whether the divergence time estimates from *fastsimcoal2* (which accounts for
306 gene flow) are in accordance with the phylogenetic topology estimated in *IQ-TREE* (which
307 does not account for gene flow). This was the case for our data: we observed deeper
308 divergence times for populations of the same ecotype compared to sister-taxa of different
309 ecotypes. For D04-H05 and D05-H06, the average divergence time between populations of
310 the same ecotype (D04-D05 and H05-H06) was 83,846 generations (SD = 3,021), whereas
311 the average divergence time between populations at each locality (D04-H05 and D05-H06)
312 was 52,569 generations (SD = 21,719). This was also true for D14-H15 and D32-H12, where
313 the average divergence time between populations of the same ecotype (D14-D32 and H12-
314 H15) was 68,723 generations (SD = 17,526), and the average divergence time between
315 populations at each locality (D14-H15 and D32-H12) was 49,882 generations (SD = 15,805).
316 Finally, we would expect that had gene flow been substantial we would observe high F_{ST}
317 values between parapatric populations, but our estimates are near 0.2.

318 Discussion

319 We have used an array of complementary approaches to disentangle the demographic history
320 of the coastal *Senecio lautus* ecotypes. In this system, many lines of evidence support a
321 multiple origin scenario for the evolution of the parapatric Dune and Headland populations.
322 The demographic history of this system reveals striking population structure and a strong

323 effect of geography and restricted dispersal, to the extent that all populations are evolving
324 largely independently from each other. Together with previous results from transplant
325 experiments (Melo et al. 2014; Richards et al. 2016; Richards and Ortiz-Barrientos 2016;
326 Walter et al. 2016; Walter, Wilkinson, et al. 2018; Wilkinson et al. 2021), our results
327 convincingly show that selection and drift, rather than gene flow, play a predominant role in
328 the genetic structure among ecotypic populations in this system. Below we discuss these
329 results considering parallel parapatric divergence in this highly replicated system.

330 **Strong genetic structure between *Senecio lautus* coastal populations**

331 Large scale genetic structure of *S. lautus* clusters populations according to their geographic
332 distribution along the Australian coast, and not by the environment they occupy. Within
333 *fastSTRUCTURE*, the largest genetic groups encompass two clades which are largely
334 independent of each other, do not show evidence of long-distance gene flow between them,
335 and also appear to contain multiple repeated instances of parapatric divergence. This genetic
336 structure, where populations group by geography and not ecology, is mirrored in the
337 phylogeny, and is consistent with our previous work using targeted sequencing of 13 neutral
338 genes (Melo et al. 2019) and RADseq using pools of individuals (Roda, Ambrose, et al.
339 2013). There is also a strong signal of isolation by distance (Wright 1943) within each
340 ecotype as well as across Dune-Headland pairs, implying long distance dispersal within the
341 system is not pervasive, which might indicate that populations are at an equilibrium between
342 dispersal and drift (Slatkin 1993). This is perhaps not surprising given that Dune and
343 Headland populations have restricted geographic ranges along the coast.

344 Fine scale genetic structure at the level of the locality (i.e., parapatric Dune-Headland
345 populations) shows that each population is genetically distinct, with little admixture, as
346 suggested by *fastSTRUCTURE* and *f3-statistics*. Despite the high potential for gene flow
347 between parapatric populations due to their close geographic proximity and relatively weak
348 F1 intrinsic reproductive isolation (Melo et al. 2014; Richards et al. 2016; Walter et al. 2016),
349 multiple transplant experiments in the system have shown that divergent natural selection is
350 strong and creates extrinsic reproductive isolation between Dune and Headland populations at
351 each locality (Melo et al. 2014; Richards et al. 2016; Richards and Ortiz-Barrientos 2016;
352 Walter et al. 2016; Walter, Wilkinson, et al. 2018; Wilkinson et al. 2021). Therefore our
353 findings are in agreement with theoretical expectations, where parapatric divergence and
354 speciation is favored when gene flow is limited and selection against immigrants and hybrids

355 is strong (Bank et al. 2012; Blanckaert and Hermisson 2018). Overall, a combination of
356 strong selection and limited dispersal can explain why parapatric populations persist despite
357 the opportunity for homogenizing gene flow between them.

358 **Parallel evolution of parapatric *S. lautus* ecotypes with minimal levels of gene flow**

359 A common doubt arising in purported cases of parallel evolution is whether gene flow is
360 responsible for the grouping of populations by geography and not by ecology (Quesada et al.
361 2007; Johannesson et al. 2010; Bierne et al. 2013; Butlin et al. 2014; Martin et al. 2015;
362 Rougemont et al. 2015; Le Moan et al. 2016; Meier et al. 2017; Pérez-Pereira et al. 2017;
363 Trucchi et al. 2017; Rougeux et al. 2019). A single origin of ecotypes combined with high
364 levels of gene flow between parapatric ecotypes at each locality can alter the phylogenetic
365 relationships of populations, falsely suggesting multiple independent origins. This is because
366 genetic structure at neutral markers can be decoupled from colonization history via
367 introgression and incomplete lineage sorting (Endler 1977; Barton and Hewitt 1985; Coyne
368 and Orr 2004; Bierne et al. 2013). This needs careful scrutiny in our system as previous work
369 showed that genomic divergence was more heterogenous in parapatric populations compared
370 to allopatric populations (Roda, Ambrose, et al. 2013), a signature of divergence with gene
371 flow (Feder and Nosil 2010; Feder et al. 2012). However, this pattern can also arise due to
372 ancestral polymorphism and incomplete lineage sorting if parapatric populations are younger
373 than allopatric populations (Cruickshank and Hahn 2014), which our current work shows.
374 Thus, processes unrelated to divergence in the face of high levels of gene flow could have
375 also contributed to the patterns of genomic divergence in this system (Roda, Ambrose, et al.
376 2013).

377 To help understand the role of gene flow during parapatric divergence in *S. lautus*, we first
378 directly estimated rates of gene flow within *fastsimcoal2*. Unexpectedly, we observed
379 minimal levels of gene flow within parapatric *S. lautus* Dune-Headland pairs. This reveals
380 that previous patterns of genomic divergence among these populations (Roda, Ambrose, et al.
381 2013) likely reflect a signature of increased genome-wide differentiation over time in
382 allopatry, and incomplete lineage sorting in parapatric populations rather than heterogeneous
383 divergence in the face of high levels of gene flow. Furthermore, we observed that most Dune-
384 Headland levels of bidirectional gene flow were similar to populations from different clades
385 and separated by greater than 1,500km, suggesting that most Dune and Headland populations
386 at each locality could be viewed as effectively allopatric. Although unmodelled changes in

387 population size tend to favor secondary contact models of gene flow (Momigliano et al.
388 2021) and our assumed genomic homogeneity of migration might affect the relative ranking
389 of demographic models (Roux et al. 2016), our estimated migration rates were consistently
390 very low across most models of gene flow (see Supplementary Table S4 for details). We do
391 not place emphasis on distinguishing between the different models of migration, but rather
392 whether parapatric divergence occurred in the presence or absence of gene flow – we are
393 confident that a small amount of gene flow has occurred between the ecotypes at most
394 localities. There are two notable exceptions (D04-H05 and D32-H12), which experience
395 levels of gene flow that would make them genetically indistinguishable ($2Nm > 1.00$) (Slatkin
396 1985a). Thus, it is still possible that gene flow has altered the observed phylogenetic
397 topology for these populations.

398 We therefore explored the conditions which are likely to obscure the history of colonization
399 by modelling the neutral divergence process through coalescent analyses and simulations in
400 *SLiM2*. We observed that the likelihood of non-monophyly is accentuated with very short
401 internal branches, which will lead to high levels of retained ancestral polymorphism and
402 therefore increase the probability that true sister taxa do not remain monophyletic; this effect
403 is largely independent of migration rates as gene flow will not contribute more to population
404 similarity beyond what ancestral polymorphism already does. Short internal branches are
405 frequently detected in systems where diversification occurs rapidly, such as in cases of
406 adaptive radiations (Schluter 2000), which seems to be the case in *S. lautus*. Our theoretical
407 approach also revealed that increasing levels of gene flow increases the likelihood of non-
408 monophyly, especially when the time of migration is further from the second population split.
409 This is because alleles introgressing into different populations will have experienced more
410 independent drift. More importantly, in these cases of secondary contact, quite high levels of
411 migration are required to create the appearance of multiple origins. Although conventional
412 thinking highlights that even small amounts of gene flow have the potential to mix
413 populations and erode their history (e.g., Endler 1977; Barton and Hewitt 1985; Coyne and
414 Orr 2004), our work suggests that this picture can be more complex in cases of secondary
415 contact involving multiple population pairs. As expected, our work reveals that it is important
416 to consider the joint contributions of gene flow as well as ancestral polymorphism when
417 inferring the likelihood of phylogenetic distortion.

418 Within *S. lautus*, even though the short internal branches and recent secondary contact have
419 the potential to obscure the phylogeny and falsely suggest parallel evolution, this is likely
420 circumvented by the extremely low rates of gene flow between most parapatric ecotypes. In
421 other words, it appears that higher amounts of gene flow would be needed to counteract the
422 divergence that has accumulated over time in the *S. lautus* system. We must also note that our
423 theoretical approach is conservative as we have ignored the effects of selection against
424 introgressed alleles. We expect that linkage to loci underlying local adaptation should act to
425 decrease the probability of a phylogeny topology switch at the locus considered. As such, a
426 polygenic basis of local adaptation could greatly reduce the probability of a topology switch
427 due to gene flow. When considering our theoretical work in combination with patterns of
428 gene flow and genetic structure in the system, there is strong evidence to suggest that *S.*
429 *lautus* populations have evolved multiple times independently.

430 Further evidence that gene flow has not obscured a single origin scenario in *S. lautus* comes
431 from comparing joint estimates of gene flow and divergence times (as implemented in
432 isolation with migration models) between population pairs of the same ecotype and putative
433 sister populations of divergent ecotypes. We observed that populations of the same ecotype
434 consistently show deeper divergence times than those from different ecotypes, which reflects
435 the topology of the phylogeny estimated in the absence of gene flow. In addition,
436 constructing the phylogeny considering gene flow (in *TreeMix*) did not alter the topology
437 from its estimation in the absence of gene flow. Although the divergences at two localities
438 (D04-H05 and D32-H12) experience levels of gene flow high enough to potentially result in
439 phylogenetic distortion, their levels of differentiation are rather high. Furthermore, each of
440 these pairs is from a separate clade and are genetically isolated from other such pairs, so even
441 moderate levels of gene flow within each pair would not have distorted the phylogeny across
442 the entire system. Together, these results imply that phylogenetic distortion is highly unlikely
443 in *S. lautus* and that such relationships reflect the true history of populations and ecotypes.

444 Additional support for the parallel evolution of *S. lautus* populations comes when considering
445 our results in combination with previous work. In *S. lautus* a clear association between
446 environment and phenotype exists in both common garden (Walter, Aguirre, et al. 2018) and
447 field conditions (James et al. 2020), as well as strong divergent selection within each
448 population pair (Melo et al. 2014; Richards et al. 2016; Richards and Ortiz-Barrientos 2016;
449 Walter et al. 2016; Walter, Wilkinson, et al. 2018; Wilkinson et al. 2021). This striking

450 association between trait and environment implies that selection would have had to
451 independently resist the introduction of maladaptive alleles to repeatedly regenerate the
452 optimal phenotype across multiple populations. Thus, parapatric systems where gene flow
453 may be extensive can still be considered 'parallel' because natural selection independently
454 maintains differentiation between ecotypes at each locality. In this manner, Lee and Coop's
455 (2019) framing of independence as an overlap in selective deaths across populations can be
456 extended to consider both the overlap in selective deaths during the initial sweep, as well as
457 during a secondary phase of resisting maladaptive gene flow. Within *S. lautus*, the current
458 and previous work provides strong support not only for the parallel origin of ecotypes, but the
459 parallel action of natural selection. Furthermore, similar phenotypes across *S. lautus* replicate
460 populations have arisen via mutations in different genes (Roda, Liu, et al. 2013; James et al.
461 2020; Wilkinson et al. 2021), providing even further evidence that natural selection would
462 have acted independently within each population. Overall, our results indicate that *S. lautus* is
463 a highly replicated system of parapatric divergences.

464 **The limits of inference from parallel evolution**

465 The *S. lautus* system allows us to study the deterministic nature of parallel evolution in
466 multiple ways. For instance, we can now begin to understand how genetic architectures vary
467 and evolve during adaptation. In doing so, we can then demonstrate whether alleles, genes or
468 pathways have been repeatedly selected for across replicate populations (Lee and Coop 2017;
469 Lee and Coop 2019). This will also help us understand whether adaptation arises from new
470 mutations or standing genetic variation (e.g., Lee and Coop 2017), or from fixation of
471 functionally equivalent alleles (such as during polygenic adaptation; Berg and Coop 2014;
472 Tiffin and Ross-Ibarra 2014; Yeaman 2015), or loss-of-function mutations (e.g., Chan et al.
473 2010). Once adaptive genes have been identified, studies of parallel evolution should directly
474 link the adaptive loci to phenotypic traits and further demonstrate that the traits themselves
475 have been under repeated selection in independent populations (Storz and Wheat 2010;
476 Pardo-Diaz et al. 2015; Hoban et al. 2016). In systems where this method is not feasible, our
477 study demonstrates that studying genome-wide loci can still uncover patterns of
478 phylogeography and migration that are consistent with parallel evolution.

479 Finally, in our work we have unusually high power to detect gene flow, as the number of
480 individuals sequenced in each of our populations is large ($N_{mean} = 57$, $2N_{mean} > 100$
481 chromosomes per population). This sampling regime allowed us to sample many rare variants

482 and therefore better distinguish ancestral polymorphism from migration. Studies undertaking
483 demographic modelling often sample 10-25 individuals per population (e.g., Roesti et al.
484 2015; Kautt et al. 2016; Trucchi et al. 2017) and occasionally even less than 10 (e.g., Meier et
485 al. 2017). Thus these studies cannot easily distinguish shared variants due to gene flow from
486 ancestral polymorphism, which can make results biased to detecting moderate to high levels
487 of gene flow, especially for recently diverged populations and in underpowered studies
488 (Slatkin 1985b; Hey and Nielsen 2007; Strasburg and Rieseberg 2010; Cruickshank and
489 Hahn 2014). As our coalescent modelling revealed that only a small amount of gene flow is
490 needed to obscure a phylogenetic topology under certain conditions (e.g., during very young
491 adaptive radiations), studies that estimate levels of gene flow with few numbers of
492 individuals and loci should treat results with caution.

493 Overall, we provide strong evidence for multiple origins of parapatric Dune and Headland
494 populations within *Senecio lautus*. Across this highly replicated system we observed
495 phylogenetic clustering by geography, strong genetic structure between populations, isolation
496 by distance, and surprisingly low gene flow between parapatric populations at each locality
497 as well as in the system as a whole. Coalescent modelling and simulations confirmed that
498 levels of gene flow are likely not high enough to obscure a single origin scenario in *S. lautus*.
499 Furthermore, the phylogenetic relationships of populations estimated in the presence of gene
500 flow agree with the main phylogeny, which supports a multiple origin scenario. These results
501 from our current work in combination with strong divergent selection between ecotypes
502 (Melo et al. 2014; Richards et al. 2016; Richards and Ortiz-Barrientos 2016; Walter et al.
503 2016; Walter, Wilkinson, et al. 2018; Wilkinson et al. 2021), strong trait-environment
504 association in the system (Walter, Aguirre, et al. 2018; James et al. 2020) and adaptation
505 across replicate populations occurring mainly via mutations in different genes (Roda, Liu, et
506 al. 2013; James et al. 2020; Wilkinson et al. 2021), implies that selection has independently
507 driven the parallel evolution of populations. This makes *S. lautus* one of the clearest
508 examples of the parallel evolution of ecotypes discovered yet, adding to the increasing
509 number of potential cases of parallel evolution in plants (Foster et al. 2007; Trucchi et al.
510 2017; Cai et al. 2019; Konečná et al. 2019). It also positions the species as a powerful system
511 of replicated parapatric divergence to study the origin of adaptation and reproductive
512 isolation.

513 # Methods

514 **Sample collection and DNA extraction**

515 Leaf samples for DNA extraction were collected from 23 Dune and Headland populations of
516 *Senecio lautus* along the coast of Australia, which included eight parapatric Dune-Headland
517 population pairs, three allopatric Headland populations, and three allopatric Dune populations
518 (n_{mean} = 58, n_{total} = 1338; Fig. 2A, Supplementary Table S5). We sampled mature (flowering)
519 plants evenly across the geographic range of each population, ensuring that sampled plants
520 were at least one meter apart. Leaf collection was undertaken with permission from the
521 Redland City Council, New South Wales National Parks and Wildlife Services (Permit
522 number: SL100215), Victoria Department of Environment and Primary Industries (Permit
523 number: 10007220), Tasmania Department of Primary Industries, Parks, Water and
524 Environment, and the Western Australia Department of Parks and Wildlife. DNA was
525 extracted using a modified CTAB protocol (Clarke 2009) and cleaned with Epoch Life
526 Sciences spin columns. We quantified sample concentration with the Invitrogen Quant-iT
527 PicoGreen dsDNA Assay Kit, and used the BioTek Take3 Micro-Volume Plate to ensure
528 DNA samples were pure. Samples were standardized to 10ng/µL.

529 **GBS library construction**

530 We created reduced representation libraries to obtain restriction site associated DNA (RAD)
531 markers. Specifically, we used a two-enzyme Genotyping-by-Sequencing (GBS) approach
532 (modified from Poland et al. 2012). We created seven libraries from the 23 Dune and
533 Headland populations, each containing 192 barcoded individuals. For each individual,
534 genomic DNA was digested with the restriction enzymes Pst1-HF (New England
535 Biosciences; NEB) and Msp1 (NEB). Forward and reverse barcodes were ligated to
536 fragments from each sample, and subsequently cleaned with homemade Serapure beads
537 (Faircloth and Glenn 2011; Rohland and Reich 2012). For each sample we amplified the
538 fragments and added Illumina sequencing primers via PCRs with 14 cycles. Each sample was
539 quantified with the Invitrogen Quant-iT PicoGreen dsDNA Assay Kit. We created seven
540 equimolar pools (192 individuals per pool), ensuring each population was evenly distributed
541 across the pools. Each pool was size-selected using the BluePippin (2% DF Marker V1, 300-
542 500bp; Sage Science), and cleaned with the Monarch PCR & DNA cleanup kit (NEB).

543 Pooled libraries were sent to the Beijing Genomics Institute (BGI) for sequencing on seven
544 lanes of the HiSeq4000, using 100bp paired-end sequencing.

545 **Reference genome**

546 A PacBio *S. lautus* reference genome (v1.0) was created from a selfing Headland individual
547 from Lennox Head (see Wilkinson et al. (2021) for additional details of the individual). The
548 plant was put in darkness for three days before young leaves were snap frozen in liquid
549 nitrogen and sent to BGI for DNA extraction and PacBio long-read sequencing (56 SMRT
550 cells). A total of 11,481,638 filtered subreads (5,072,756 from RSII sequencer and 6,408,882
551 from Sequel sequencer) were used with a mean read length of ~8K base pairs and an
552 expected genome coverage of ~60X. The genome was de novo assembled using CANU
553 1.6 (REF) with default settings. The final assembly consisted of 60,947 contigs with an N50
554 of 34K. The BUSCO gene content completeness was 86% (4% fragmented and 10%
555 missing).

556 **Bioinformatics**

557 For the GBS sequencing, BGI removed forward barcodes and quality filtered the raw reads to
558 remove reads containing Illumina adaptors, low quality reads (> 50% of bases < Q10), and
559 reads with > 10% Ns. We trimmed reverse barcodes with *TagCleaner* standalone v0.12
560 (Schmieder et al. 2010). We retained an average of 2,849,159 clean reads (SD = 827,036)
561 across the 1,319 individuals (after the removal of 19 individuals with high levels of missing
562 data, see below; Supplementary Table S6). Reads were mapped to the *S. lautus* reference
563 PacBio genome v1.0 with *BWA-MEM* v0.7.15 (Li and Durbin 2009; Li 2013). On average,
564 86% of reads (SD = 15) mapped to the reference genome, and 81% (SD = 15) mapped
565 properly with their paired-read (Supplementary Table S6). *PicardTools* v2.7.0 (Broad
566 Institute 2019) was used to clean aligned reads and to add read groups (PCR duplicates were
567 not marked for removal). We jointly called all variant and invariant sites for each population
568 with *FreeBayes* v1.1.0 (Garrison and Marth 2012). Because SNPs were separately called for
569 each of the 23 populations, we first normalized the 23 VCF files before merging them
570 together. This was achieved by first using BCFtools v1.4.1 (Li et al. 2009) to split multiallelic
571 sites into biallelic records. Each file was then normalized by re-joining biallelic sites into
572 multiallelic records. We then left-aligned and normalized indels, and used *vt* (Tan et al. 2015)

573 to decompose biallelic block substitutions into separate SNPs for each population. We
574 merged the 23 per-population VCF files into one large file for subsequent SNP filtering.

575 We largely followed the *dDocent* pipeline for SNP filtering (Puritz, Hollenbeck, et al. 2014;
576 Puritz, Matz, et al. 2014), including iterative filtering to maximize the number of sampled
577 SNPs (O'Leary et al. 2018). Using *VCFtools* v0.1.15 (Danecek et al. 2011), we first retained
578 sites if they were present in > 50% of individuals, had a minimum quality score of 30, and a
579 minimum minor allele count of 1. We filtered for a minimum depth of 3 for a genotype call.
580 Individuals were removed if they contained > 40% missing data. We then filtered for a
581 maximum mean depth of 100, and a minimum mean depth of 10. We filtered for missing data
582 per population, removing sites if they contained > 50% of missing data within each
583 population. We refiltered for an overall missing data of 20%. Indels were removed with *vcflib*
584 (Garrison 2016). We then filtered for population-specific Hardy Weinberg Equilibrium using
585 the *filter_hwe_by_pop.pl* script within *dDocent*. See below for the minor allele frequency
586 thresholds for each analysis.

587 **Do populations cluster by geography or ecotype?**

588 To explore the broad patterns of genetic clustering of populations, we performed two separate
589 analyses: phylogeny construction and *fastSTRUCTURE* (Raj et al. 2014). We used *PLINK*
590 v1.9 (Purcell et al. 2007) to remove SNPs with a minor allele frequency (MAF) of < 0.05,
591 and also to thin SNPs by retaining one unlinked SNP per RAD locus. This dataset contained
592 3,844 unlinked SNPs across the 1,319 individuals. We generated a maximum likelihood
593 phylogeny within *IQ-TREE* v1.6.0 (Nguyen et al. 2015) using the polymorphisms-aware
594 phylogenetic model (Schrempf et al. 2016). We first used ModelFinder (Kalyaanamoorthy et
595 al. 2017) to determine the best-fit substitution model for the data (TVMe+FQ+P+N9+G4),
596 and increased the virtual population size (N) to the maximum value of 19 (as recommended
597 by Schrempf et al. 2016). Default parameters were used for tree construction, with the
598 western Australia D09 population assigned as the outgroup. To assess convergence, we
599 undertook 10 separate runs of *IQ-TREE* and examined tree topology (which remained
600 unchanged across the 10 independent runs). We also ensured that the log-likelihood values
601 were stable at the end of each run. Branch support was performed using 10,000 replicates of
602 UFboot (Hoang et al. 2018), and 10,000 replicates of SH-aLRT (Guindon et al. 2010).

603 We further explored broad patterns of population structure using the variational Bayesian
604 framework, *fastSTRUCTURE* v1.0 (Raj et al. 2014). Here, we implemented *fastSTRUCTURE*
605 to provide extra evidence for whether populations genetically cluster by geography or
606 ecotype. We did not infer specific historical admixture scenarios from *fastSTRUCTURE*, as
607 different demographic scenarios can give rise to indistinguishable structure plots (Lawson et
608 al. 2018). The *fastSTRUCTURE* algorithm assigns individuals into genetic clusters (K) by
609 minimizing departures from Hardy-Weinberg equilibrium and inferring individual ancestry
610 proportions to each genetic cluster. We followed the recommendations by Gilbert et al.
611 (2012) and Janes et al. (2017) and ran the simple prior (K=1-30) with 100 independent runs
612 per K-value. In order to determine the most likely number of genetic clusters (the optimal K),
613 we used the *chooseK.py* script from *fastSTRUCTURE* to examine (1) the K-value that best
614 explained the structure in the data (the smallest number of model components that accounted
615 for almost all of the ancestry in the sample), and (2) the K-value that maximized the marginal
616 likelihood of the data. Results were summarized and plotted in the R package *pophelper*
617 v2.2.7 (Francis 2017).

618 **Has gene flow shaped patterns of divergence across the system?**

619 To explore patterns of gene flow in a phylogenetic context, we used *TreeMix* v1.13 (Pickrell
620 and Pritchard 2012). *TreeMix* constructs a bifurcating maximum likelihood tree, identifies
621 populations that are poor fits to the model, and sequentially adds migration events that
622 improve the fit of the data. SNPs for which MAF < 0.01 were filtered, which retained 24,933
623 SNPs across the 1,319 individuals. We constructed an initial 25 maximum likelihood trees
624 with no migration, 1,000 bootstrap replicates in blocks of 50 SNPs with D09 as the assigned
625 outgroup, and selected the tree with the highest log-likelihood as the input tree for all
626 subsequent analyses. We then tested between 1-25 migration events in blocks of 50 SNPs.
627 Trees and migration events were robust to varying the size of the linkage blocks as well as
628 the MAF threshold of the dataset (data not shown). To select the number of migration events,
629 we examined the log-likelihoods and cumulative variance explained by each model, and
630 performed jackknife estimates to obtain the standard error and significance of the weight of
631 each migration event. However, the interpretation of these P-values should be treated with
632 caution due to possible errors in the tree structure as well as the inference of incorrect
633 migration events (Pickrell and Pritchard 2012).

634 To more formally test for genetic admixture, we used the *threepop* function in *TreeMix* to
635 calculate *f3*-statistics (Reich et al. 2009). The *f3*-statistic determines whether a particular
636 population (*A*) is the result of admixture between two other populations (*B* and *C*). It
637 measures the difference in allele frequencies between populations *A* and *B*, and populations *A*
638 and *C*. Only when admixture is present, do we expect the allele frequency of population *A* to
639 be intermediate between the allele frequencies of populations *B* and *C*. In contrast, in the
640 absence of gene flow, the allele frequency of population *A* should not be consistently
641 intermediate between *B* and *C*. Therefore, *f3* can be interpreted as the amount of shared
642 genetic drift between two populations from a common ancestor. In the absence of admixture,
643 *f3* (*A*; *B*, *C*) will be positive, whereas a significantly negative value of *f3* provides evidence
644 for *A* being admixed from *B* and *C*. We calculated *f3* for all possible triads of populations
645 with jackknifing in blocks of 50 SNPs to obtain Z-scores for calculating statistical
646 significance (Z-score < -3.8 = P < 0.0001).

647 The erect phenotype is common across Australian species of the genus *Senecio* (Thompson
648 2005), except for the prostrate *S. lautus* Headland ecotype and a few Alpine populations,
649 suggesting these prostrate forms are derived. We tested for isolation by distance (IBD;
650 Wright 1943) in the ancestral and derived ecotypes to evaluate similarities in their dispersal
651 dynamics (Slatkin 1993). We tested for IBD using migration rates (2*Nm*) inferred in
652 *fastsimcoal2* (see below) as well as Slatkin's $\widehat{M}$, $(1 / F_{ST} - 1)/4$, as a proxy for gene flow
653 (Slatkin 1993). For Slatkin's $\widehat{M}$, we excluded the Western Australia populations (D09 and
654 D35), and SNPs for which MAF < 0.05 were filtered. We calculated pairwise F_{ST} in
655 VCFtools. We calculated pairwise geographic distances using the following formula, which
656 uses the spherical law of cosines to consider the curvature of the earth:

657 $$6378137 \times \mathrm{acos}(\sin(lat_1) \times \sin(lat_2) + \cos(lat_1) \times \cos(lat_2) \times \cos(long_1 - long_2))$$

658 where: 6378137 is earth's radius in meters, and *lat* and *long* are the latitude and longitude (in
659 radians) of the two populations being compared. For the *fastsimcoal2* migration rates, we
660 tested for IBD between the Dune and Headland within each population pair using a linear
661 model in R v3.4.2 (R Core Team 2017), using an average of the bidirectional gene flow rates
662 for each pair (log-log scale). For Slatkin's $\widehat{M}$, we also tested for IBD between the Dune and
663 Headland of each population pair (log-log scale) using a linear model in R, and tested for
664 IBD within the Dunes, and within the Headlands (log-log scale) using Mantel tests with
665 9,999 permutations in R (*mantel* function in the *vegan* package; Blanchet et al. 2018).

666 **Is there gene flow between parapatric populations?**

667 We examined levels of admixture between parapatric populations with *STRUCTURE* v2.3.4
668 (Pickrell and Pritchard 2012). *STRUCTURE* is a Bayesian MCMC approach that assigns
669 populations into genetic clusters (K) based on individual genotypes by assuming Hardy-
670 Weinberg Equilibrium within a population. It assigns each individual an admixture
671 coefficient to depict the proportion of the genome that originated from a particular K cluster.
672 To increase the numbers of SNPs, we took a subset of the data by excluding the two
673 populations from the west coast of Australia (D09 and D35). Excluding these most divergent
674 populations decreased the amount of missing data and thus increased the number of common
675 SNPs in the south-eastern populations. We used the same filtering procedure as above,
676 removed SNPs with MAF < 0.05 and thinned SNPs in *PLINK* to retain one SNP per RAD
677 locus. Each Dune-Headland population pair was extracted, and SNPs with MAF < 0.05 were
678 filtered. We retained between 837 and 2,606 unlinked SNPs per pair (mean = 1,905 SNPs;
679 SD = 575). *STRUCTURE* analysis was run using the admixture model and the correlated
680 allele frequency model (Falush et al. 2003) with 10 independent runs for K=1-6 (50,000
681 burn-in and 200,000 MCMC iterations). We visually inspected summary statistics of MCMC
682 runs to ensure convergence of model parameters. As we were specifically interested in
683 detecting admixed individuals between the two ecotypes, we plotted results for K=2. To
684 explore any additional genetic structure within a pair, we also estimated the optimal K-value
685 with the Evanno method (Evanno et al. 2005), by examining the maximum value for ΔK (the
686 second order rate of change in the log probability of data between successive K-values). The
687 R package *pophelper* was used to calculate the ΔK, summarize results and plot the data.

688 We directly estimated levels of gene flow between population pairs from the site frequency
689 spectrum (SFS) using the composite-likelihood method implemented in *fastsimcoal2* v2.6.0.3
690 (Excoffier et al. 2013). The joint SFS of two populations is sensitive to demographic
691 processes. For instance, gene flow will result in more low-frequency shared polymorphisms
692 than expected under a non-migration scenario (Hahn 2018). We tested ten demographic
693 models (Fig. 4B), and inferred migration rates, as well as other demographic parameters
694 including current and past population sizes, ancestral population size, divergence time, time
695 of secondary contact, and gene flow cessation time, for eight Dune-Headland (DH)
696 population pairs. We additionally asked whether gene flow was occurring in a linear fashion
697 down the coast within each ecotype by testing eight Dune-Dune (DD) and eleven Headland-

698 Headland (HH) pairs. To determine the baseline level of gene flow inferred by *fastsimcoal2*
699 between isolated populations, namely the null gene flow expectation, we estimated migration
700 rates for three very divergent allopatric populations (>1,500km apart, between the eastern and
701 south-eastern clades; D03-D32, D03-H12, and H02-H12), and took the highest detected
702 migration rate from these allopatric comparisons as the baseline migration rate.

703 As above, the Western Australia populations (D09 and D35) were excluded from this dataset
704 to increase the number of sampled SNPs. For each pair, we filtered for a minor allele count of
705 one (MAC1), retaining between 6,679 and 19,951 variable sites per pair (mean = 12,155
706 SNPs, SD = 3,316). By using a MAC1 and a relatively high number of samples per
707 population (mean = 57, SD = 15), we retained rare alleles that are informative about
708 migration events between the populations (Slatkin 1985b). We note that we also ran
709 *fastimcoal2* removing SNPs with MAF < 0.05. We found that migration rates were higher
710 using MAC1 compared to MAF0.05 which means that if anything, we would be
711 overestimating migration rates, which would make our case for very low gene flow even
712 stronger (result not shown). Since we cannot distinguish ancestral from derived alleles, we
713 used the minor allele SFS (folded SFS). We used an *ad hoc* approach to estimate the number
714 of monomorphic sites (Supplementary Methods S1). Gene flow estimates were robust to
715 varying the number of monomorphic sites (data not shown). We generated the joint folded
716 SFS per population pair without downsampling using *vcf2dadi* and *dadi2fsc.2pop* R functions
717 from Liu et al. (2018). See Supplementary Table S4 for details on the number of SNPs,
718 number of monomorphic sites and models tested for each pair comparison.

719 We performed 50 independent *fastsimcoal2* runs per model per population pair. Each run
720 consisted of 100,000 coalescent simulations and 40 expectation-maximization cycles for
721 parameter optimization. We used a mutation rate of 1.0×10^{-8} based on Asteraceae EST
722 sequence comparisons and fossil calibrations (Strasburg and Rieseberg 2008). We ranked the
723 models based on the Kullback–Leibler information value which was estimated from the
724 Akaike information criterion (AIC) scores of the best run per model. Here, the normalization
725 of the difference between the AIC scores of a particular model and the best model in the set
726 provides a measure of the degree of support for a particular model, namely model likelihood
727 (w_i) (Thomé and Carstens 2016). Since the use of linked-SNPs might lead to pseudo-
728 replication issues when comparing models based on *fastsimcoal2* likelihood values (Bagley et

729 al. 2017) and the SFS discards linkage information, we verified SNPs were largely unlinked
730 by calculating linkage-disequilibrium in PLINK (data not shown).

731 As *fastsimcoal2* uses simulations to approximate the likelihood values, there is variance in
732 the likelihood estimates. To test whether the best model significantly differs from alternative
733 models with very low gene flow ($2Nm = 0.01$) but the same values at other parameters, we
734 compared their likelihood distributions based on 100 expected SFS from 100,000 coalescent
735 simulations per model (Bagley et al. 2017). If likelihood distributions overlap, there is no
736 significant differences between the fit of both models (Meier et al. 2017). To obtain
737 confidence intervals for all demographic parameters, we performed parametric bootstrapping.
738 Given the parameter values of the best run of the best model, we simulated 100 SFS and re-
739 estimated the parameter values from them. Each run consisted of 100,000 coalescent
740 simulations and 30 expectation-maximization cycles. The parameter values of the best run of
741 the best model were specified as the initial values of each bootstrapping run. We computed
742 the 95% confidence intervals of all parameters with the *groupwiseMean* function of
743 *rcompanion* R package (Mangiafico 2015).

744 **Is gene flow high enough to obscure a single origin scenario?**

745 To better understand under what conditions gene flow can erode a signal of phylogenetic
746 monophyly of each ecotype, we created a coalescent model to represent a single origin
747 scenario of ecotypes within *Mathematica* v12.2 (Wolfram Research, Inc. 2020) (see
748 Supplementary Methods S2 for full details). We assumed a species tree consisting of four
749 populations, with two sets of sister taxa to represent populations of the same ecotype (Fig.
750 5A). The ancestor of the ecotypes splits at time $t2$ in the past, and we can think of this split as
751 an initial single origin of the Dune and Headland ecotypes. To represent two parapatric
752 population pairs, each of these two ecotypes further split simultaneously at time, $t1$, in the
753 past. We considered an instantaneous burst of migration from the populations of the ancestral
754 ecotype into the populations of the derived ecotype at each locality by assuming that a
755 fraction, m, of alleles in each derived ecotype population is replaced by migrant alleles from a
756 parapatric population at time, tm, in the past. Considering a single lineage from each of the
757 four populations starting at the present, we condition on the migrant status of the sampled
758 lineages to calculate coalescent probabilities of gene tree topologies that result in a grouping
759 in which the two populations of the derived ecotype are not monophyletic in the gene
760 genealogy. These methods recapitulate recent more formal treatments of the probability of

761 hemiplasy (non-monophyly despite a single mutational origin for a trait) under incomplete
762 lineage sorting and introgression (Guerrero and Hahn 2018; Hibbins et al. 2020), though we
763 have considered a scenario involving four populations to reflect the nature of parapatric pairs.
764 Moreover, our emphasis is placed on the implications of gene flow for the original inference
765 of the species tree itself, rather than how it pertains to the history of a selected locus of
766 interest under an inferred phylogeny. Furthermore, we ran forward simulations of neutral
767 polymorphism in *SLiM2* (Haller and Messer 2017) to further gain insight into the conditions
768 in which gene flow can distort the phylogenetic topology. Instead of having an instantaneous
769 unidirectional burst of migration, we considered a scenario of continuous and symmetrical
770 migration. See Supplementary Methods S3-S5 for full description of the approach used.

771 Finally, although we cannot directly map where our observed data fall in the simulated
772 parameter space, we can gain further confidence on the likelihood of phylogenetic distortion
773 by considering divergence time estimates from *fastsimcoal2* in combination with the
774 phylogenetic topology estimated in *IQ-TREE*. More specifically, we asked whether
775 divergence times between populations from the same ecotype are deeper than between
776 populations from different ecotypes. The estimation of divergence times in *fastsimcoal2*
777 considers gene flow, thus if they are in accordance with relative node order of the *IQ-TREE*
778 phylogeny (which is estimated without accounting for gene flow), it suggests that
779 phylogenetic distortion within the system is unlikely. We thus compared the *fastsimcoal2*
780 divergence times to the relative node order of the *IQ-TREE* phylogeny for four population
781 pairs (D04-H05 and D05-H06; D14-H15 and D32-H12). We selected these pairs because
782 they represent neighboring sister-taxa within the phylogeny.

783 Acknowledgements

784 We are grateful to M.J. Wilkinson, H.N. Nguyen Vu and H.L. North for assisting with
785 sample collection. We extend our thanks to R.K. Bagley for assisting with *fastsimcoal2*. We
786 thank Ortiz-Barrientos laboratory members for insightful comments on previous versions of
787 this manuscript. S. Chenoweth and M. Blows provided very useful feedback on M.E. James'
788 PhD dissertation. This work was supported by an Australian Research Council grant
789 (DP190103039) to D.O. and J.E., and a University of Queensland Graduate School
790 International Travel Award to M.E.J.

Author contributions

M.E.J and D.O. conceived the project. M.E.J. and J.E. undertook sample collection. M.E.J. extracted DNA, prepared libraries, performed bioinformatics, and undertook the *IQ-TREE*, *fastSTRUCTURE*, *STRUCTURE* and *TreeMix* analyses. S.LA. assembled the reference genome. H.A. conducted the *fastsimcoal2* analyses. J.S.G. performed the coalescent modelling and *SLiM2* simulations with input from J.E. The paper was written by M.E.J. and D.O. with input from all authors. D.O. is the mentor and supervisor for the research program.

Data and code availability

The data and code underlying this article are available in GitHub, at https://github.com/OB-lab/James_et_al._2021-MBE.

References

Ali S. 1964. *Senecio lautus* complex in Australia. I. Taxonomic considerations and discussion of some of the related taxa from New Zealand. *Aust. J. Bot.* 12:282–291.

Allender CJ, Seehausen O, Knight ME, Turner GF, Maclean N. 2003. Divergent selection during speciation of Lake Malawi cichlid fishes inferred from parallel radiations in nuptial coloration. *PNAS* 100:14074–14079.

Bagley RK, Sousa VC, Niemiller ML, Linnen CR. 2017. History, geography and host use shape genomewide patterns of genetic variation in the redheaded pine sawfly (*Neodiprion lecontei*). *Mol. Ecol.* 26:1022–1044.

Bank C, Bürger R, Hermisson J. 2012. The limits to parapatric speciation: Dobzhansky–Muller Incompatibilities in a continent–island model. *Genetics* 191:845–863.

Barton NH, Hewitt GM. 1985. Analysis of hybrid zones. *Annu. Rev. Ecol. Syst.* 16:113–148.

Beardsley PM, Schoenig SE, Whittall JB, Olmstead RG. 2004. Patterns of evolution in western North American *Mimulus* (Phrymaceae). *Am. J. Bot.* 91:474–489.

Berg JJ, Coop G. 2014. A population genetic signal of polygenic adaptation. *PLoS Genet.* 10:e1004412.

Berglund ABN, Dahlgren S, Westerbergh A. 2003. Evidence for parallel evolution and site-specific selection of serpentine tolerance in *Cerastium alpinum* during the colonization of Scandinavia. *New Phytol.* 161:199–209.

Bierne N, Gagnaire PA, David P. 2013. The geography of introgression in a patchy environment and the thorn in the side of ecological speciation. *Curr. Zool.* 59:72–86.

Blanchet G, Friendly M, Kindt R, Legendre P, McGlinn D, Minchin PR, O'Hara RB, Simpson GL, Solymos P, Stevens MHH, et al. 2018. vegan: Community Ecology Package. R package version 2.5-2. https://CRAN.R-project.org/package=vegan

Blanckaert A, Hermisson J. 2018. The limits to parapatric speciation II: Strengthening a preexisting genetic barrier to gene flow in parapatry. *Genetics* 209:241–254.

Blount ZD, Lenski RE, Losos JB. 2018. Contingency and determinism in evolution: Replaying life's tape. *Science* 362:eaam5979.

Bolnick DI, Barrett RDH, Oke KB, Rennison DJ, Stuart YE. 2018. (Non)Parallel evolution. *Annu. Rev. Ecol. Evol. Syst.* 49:303–330.

Broad Institute. 2019. PicardTools. GitHub Repository. http://broadinstitute.github.io/picard/

Butlin RK, Saura M, Charrier G, Jackson B, André C, Caballero A, Coyne JA, Galindo J, Grahame JW, Hollander J, et al. 2014. Parallel evolution of local adaptation and reproductive isolation in the face of gene flow. *Evolution* 68:935–949.

Cai Z, Zhou L, Ren NN, Xu X, Liu R, Huang L, Zheng X-M, Meng Q-L, Du Y-S, Wang M-X, et al. 2019. Parallel speciation of wild rice associated with habitat shifts. *Mol. Biol. Evol.* 36:875–889.

Chan YF, Marks ME, Jones FC, Villarreal G, Shapiro MD, Brady SD, Southwick AM, Absher DM, Grimwood J, Schmutz J, et al. 2010. Adaptive evolution of pelvic reduction in sticklebacks by recurrent deletion of a Pitx1 enhancer. *Science* 327:302–305.

Clarke JD. 2009. Cetyltrimethyl Ammonium Bromide (CTAB) DNA miniprep for plant DNA isolation. *Cold Spring Harb. Protoc.* 2009:Pdb.prot5177.

Colosimo PF, Hosemann KE, Balabhadra S, Villarreal G, Dickson M, Grimwood J, Schmutz J, Myers RM, Schluter D, Kingsley DM. 2005. Widespread parallel evolution in sticklebacks by repeated fixation of Ectodysplasin alleles. *Science* 307:1928–1933.

Coyne JA, Orr HA. 2004. Speciation. Sunderland: Sinauer Associates

Cruickshank TE, Hahn MW. 2014. Reanalysis suggests that genomic islands of speciation are due to reduced diversity, not reduced gene flow. *Mol. Ecol.* 23:3133–3157.

Danecek P, Auton A, Abecasis G, Albers CA, Banks E, DePristo MA, Handsaker RE, Lunter G, Marth GT, Sherry ST, et al. 2011. The variant call format and VCFtools. *Bioinformatics* 27:2156–2158.

Elmer KR, Kusche H, Lehtonen TK, Meyer A. 2010. Local variation and parallel evolution: morphological and genetic diversity across a species complex of neotropical crater lake cichlid fishes. *Philos. Trans. R. Soc. B* 365:1763–1782.

Endler J. 1977. Geographic variation, speciation, and clines. Princeton: Princeton University Press

Evanno G, Regnaut S, Goudet J. 2005. Detecting the number of clusters of individuals using the software structure: a simulation study. *Mol. Ecol.* 14:2611–2620.

Excoffier L, Dupanloup I, Huerta-Sánchez E, Sousa VC, Foll M. 2013. Robust demographic inference from genomic and SNP data. *PLoS Genet.* 9:e1003905.

Faircloth B, Glenn T. 2011. Serapure. https://ethanomics.files.wordpress.com/2012/08/serapure_v2-2.pdf

Falush D, Stephens M, Pritchard JK. 2003. Inference of population structure using multilocus genotype data: linked loci and correlated allele frequencies. *Genetics* 164:1567–1587.

Feder JL, Egan SP, Nosil P. 2012. The genomics of speciation-with-gene-flow. *Trends Genet.* 28:342–350.

Feder JL, Nosil P. 2010. The efficacy of divergence hitchhiking in generating genomic islands during ecological speciation. *Evolution* 64:1729–1747.

Foster SA, McKinnon GE, Steane DA, Potts BM, Vaillancourt RE. 2007. Parallel evolution of dwarf ecotypes in the forest tree *Eucalyptus globulus*. *New Phytol.* 175:370–380.

Francis RM. 2017. POPHELPER: an R package and web app to analyse and visualize population structure. *Mol. Ecol. Resour.* 17:27–32.

Freeman S, Herron J. 2004. Evolutionary Analysis. 4th ed. Upper Saddle River, NJ: Pearson/Prentice Hall

Garrison E. 2016. Vcflib, a simple C++ library for parsing and manipulating VCF files. https://github.com/vcflib/vcflib

Garrison E, Marth G. 2012. Haplotype-based variant detection from short-read sequencing. :arXiv. arXiv:1207.3907v2 [q-bio.GN].

Gilbert KJ, Andrew RL, Bock DG, Franklin MT, Kane NC, Moore J-S, Moyers BT, Renaut S, Rennison DJ, Veen T, et al. 2012. Recommendations for utilizing and reporting population genetic analyses: the reproducibility of genetic clustering using the program STRUCTURE. *Mol. Ecol.* 21:4925–4930.

Guerrero RF, Hahn MW. 2018. Quantifying the risk of hemiplasy in phylogenetic inference. *PNAS* 115:12787–12792.

Guindon S, Dufayard JF, Lefort V, Anisimova M, Hordijk W, Gascuel O. 2010. New algorithms and methods to estimate maximum-likelihood phylogenies: Assessing the performance of PhyML 3.0. *Syst. Biol.* 59:307–321.

Hahn MW. 2018. Molecular population genetics. Sunderland: Sinauer Associates

Haller BC, Messer PW. 2017. SLiM 2: Flexible, interactive forward genetic simulations. *Mol. Biol. Evol.* 34:230–240.

Herman A, Brandvain Y, Weagley J, Jeffery WR, Keene AC, Kono TJY, Bilandžija H, Borowsky R, Espinasa L, O'Quin K, et al. 2018. The role of gene flow in rapid and repeated evolution of cave-related traits in Mexican tetra, *Astyanax mexicanus*. *Mol. Ecol.* 27:4397–4416.

Hey J, Nielsen R. 2007. Integration within the Felsenstein equation for improved Markov chain Monte Carlo methods in population genetics. *PNAS* 104:2785–2790.

Hibbins MS, Gibson MJ, Hahn MW. 2020. Determining the probability of hemiplasy in the presence of incomplete lineage sorting and introgression. *eLife* 9:e63753.

Hoang DT, Chernomor O, von Haeseler A, Minh BQ, Vinh LS. 2018. UFBoot2: Improving the ultrafast bootstrap approximation. *Mol. Biol. Evol.* 35:518–522.

Hoban S, Kelley JL, Lotterhos KE, Antolin MF, Bradburd G, Lowry DB, Poss ML, Reed LK, Storfer A, Whitlock MC. 2016. Finding the genomic basis of local adaptation: pitfalls, practical solutions, and future directions. *Am. Nat.* 188:379–397.

James ME, Wilkinson MJ, North HL, Engelstädter J, Ortiz-Barrientos D. 2020. A framework to quantify phenotypic and genotypic parallel evolution. Preprint at https://doi.org/10.1101/2020.02.05.936450.

Janes JK, Miller JM, Dupuis JR, Malenfant RM, Gorrell JC, Cullingham CI, Andrew RL. 2017. The *K* = 2 conundrum. *Mol. Ecol.* 26:3594–3602.

Johannesson K, Panova M, Kemppainen P, André C, Rolán-Alvarez E, Butlin RK. 2010. Repeated evolution of reproductive isolation in a marine snail: unveiling mechanisms of speciation. *Philos. Trans. R. Soc. B* 365:1735–1747.

Kalyaanamoorthy S, Minh BQ, Wong TKF, von Haeseler A, Jermiin LS. 2017. ModelFinder: fast model selection for accurate phylogenetic estimates. *Nat. Methods* 14:587–589.

Kautt AF, Machado-Schiaffino G, Meyer A. 2016. Multispecies outcomes of sympatric speciation after admixture with the source population in two radiations of Nicaraguan crater lake cichlids. *PLoS Genet.* 12:e1006157.

Konečná V, Nowak MD, Kolář F. 2019. Parallel colonization of subalpine habitats in the central European mountains by *Primula elatior*. *Sci. Rep.* 9:3294.

Lawson DJ, van Dorp L, Falush D. 2018. A tutorial on how not to over-interpret STRUCTURE and ADMIXTURE bar plots. *Nat. Commun.* 9:3258.

Le Moan A, Gagnaire PA, Bonhomme F. 2016. Parallel genetic divergence among coastal-marine ecotype pairs of European anchovy explained by differential introgression after secondary contact. *Mol. Ecol.* 25:3187–3202.

Lee KM, Coop G. 2017. Distinguishing among modes of convergent adaptation using population genomic data. *Genetics* 207:1591–1619.

Lee KM, Coop G. 2019. Population genomics perspectives on convergent adaptation. *Philos. Trans. R. Soc. B* 374:20180236.

Lenormand T, Chevin LM, Bataillon T. 2016. Parallel evolution: what does it (not) tell us and why is it (still) interesting? In: Chance in Evolution. Chicago: University Chicago Press.

Li H. 2013. Aligning sequence reads, clone sequences and assembly contigs with BWA-MEM. :arXiv:1303.3997 [q-bio.GN].

Li H, Durbin R. 2009. Fast and accurate short read alignment with Burrows-Wheeler transform. *Bioinformatics* 25:1754–1760.

Li H, Handsaker B, Wysoker A, Fennell T, Ruan J, Homer N, Marth G, Abecasis G, Durbin R, 1000 Genome Project Data Processing Subgroup. 2009. The Sequence Alignment/Map format and SAMtools. *Bioinformatics* 25:2078–2079.

Liu S, Ferchaud AL, Grønkjaer P, Nygaard R, Hansen MM. 2018. Genomic parallelism and lack thereof in contrasting systems of three-spined sticklebacks. *Mol. Ecol.* 27:4725–4743.

Magalhaes IS, Whiting JR, D'Agostino D, Hohenlohe PA, Mahmud M, Bell MA, Skúlason S, MacColl ADC. 2020. Intercontinental genomic parallelism in multiple three-spined stickleback adaptive radiations. *Nat. Ecol. Evol.*:1–11.

Mangiafico S S. 2015. An R companion for the handbook of biological statistics. https://rcompanion.org/rcompanion/

Martin CH, Cutler JS, Friel JP, Dening Touokong C, Coop G, Wainwright PC. 2015. Complex histories of repeated gene flow in Cameroon crater lake cichlids cast doubt on one of the clearest examples of sympatric speciation. *Evolution* 69:1406–1422.

Meier JI, Sousa VC, Marques DA, Selz OM, Wagner CE, Excoffier L, Seehausen O. 2017. Demographic modelling with whole-genome data reveals parallel origin of similar *Pundamilia* cichlid species after hybridization. *Mol. Ecol.* 26:123–141.

Melo MC, Grealy A, Brittain B, Walter GM, Ortiz-Barrientos D. 2014. Strong extrinsic reproductive isolation between parapatric populations of an Australian groundsel. *New Phytol.* 203:323–334.

Melo MC, James ME, Roda F, Bernal-Franco D, Wilkinson MJ, Liu H, Walter GM, Ortiz-Barrientos D. 2019. Evidence for mutation-order speciation in an Australian wildflower. Preprint at https://doi.org/10.1101/692673.

Momigliano P, Florin A-B, Merilä J. 2021. Biases in demographic modelling affect our understanding of recent divergence. *Mol. Biol. Evol.* Advanced access, doi:10.1093.

Nelson TC, Stathos AM, Vanderpool DD, Finseth FR, Yuan Y, Fishman L. 2021. Ancient and recent introgression shape the evolutionary history of pollinator adaptation and speciation in a model monkeyflower radiation (*Mimulus* section *Erythranthe*). *PLoS Genet.* 17:e1009095.

Nguyen LT, Schmidt HA, von Haeseler A, Minh BQ. 2015. IQ-TREE: A fast and effective stochastic algorithm for estimating maximum-likelihood phylogenies. *Mol. Biol. Evol.* 32:268–274.

O'Leary SJ, Puritz JB, Willis SC, Hollenbeck CM, Portnoy DS. 2018. These aren't the loci you're looking for: Principles of effective SNP filtering for molecular ecologists. *Mol. Ecol.* 27:3193–3206.

Orr HA. 2005. The probability of parallel evolution. *Evolution* 59:216–220.

Ostevik KL, Moyers BT, Owens GL, Rieseberg LH. 2012. Parallel ecological speciation in plants? *Int. J. Ecol.* 2012:1–17.

Pardo-Diaz C, Salazar C, Jiggins CD. 2015. Towards the identification of the loci of adaptive evolution. *Methods Ecol. Evol.* 6:445–464.

Pérez-Pereira N, Quesada H, Caballero A. 2017. Can parallel ecological speciation be detected with phylogenetic analyses? *Mol. Phylogenet. Evol.* 116:149–156.

Perreault-Payette A, Muir AM, Goetz F, Perrier C, Normandeau E, Sirois P, Bernatchez L. 2017. Investigating the extent of parallelism in morphological and genomic divergence among lake trout ecotypes in Lake Superior. *Mol. Ecol.* 26:1477–1497.

Pickrell JK, Pritchard JK. 2012. Inference of population splits and mixtures from genome-wide allele frequency data. *PLoS Genet.* 8:e1002967.

Poland JA, Brown PJ, Sorrells ME, Jannink JL. 2012. Development of high-density genetic maps for barley and wheat using a novel two-enzyme Genotyping-by-Sequencing approach. *PLoS ONE* 7:e32253.

Pritchard JK, Stephens M, Donnelly P. 2000. Inference of population structure using multilocus genotype data. *Genetics* 155:945–959.

Purcell S, Neale B, Todd-Brown K, Thomas L, Ferreira MAR, Bender D, Maller J, Sklar P, de Bakker PIW, Daly MJ, et al. 2007. PLINK: A tool set for whole-genome association and population-based linkage analyses. *Am. J. Hum. Genet.* 81:559–575.

Puritz JB, Hollenbeck CM, Gold JR. 2014. *dDocent*: a RADseq, variant-calling pipeline designed for population genomics of non-model organisms. *PeerJ* 2:e431.

Puritz JB, Matz MV, Toonen RJ, Weber JN, Bolnick DI, Bird CE. 2014. Demystifying the RAD fad. *Mol. Ecol.* 23:5937–5942.

Quesada H, Posada D, Caballero A, Morán P, Rolán-Alvarez E. 2007. Phylogenetic evidence for multiple sympatric ecological diversification in a marine snail. *Evolution* 61:1600–1612.

R Core Team. 2017. R: A language and environment for statistical computing. R Foundation for Statistical Computing. Vienna, Austria. https://www.R-project.org/

Radford IJ, Cousens RD, Michael PW. 2004. Morphological and genetic variation in the *Senecio pinnatifolius* complex: are variants worthy of taxonomic recognition? *Aust. Syst. Bot.* 17:29–48.

Raj A, Stephens M, Pritchard JK. 2014. fastSTRUCTURE: Variational inference of population structure in large SNP data sets. *Genetics* 197:573–589.

Ravinet M, Prodöhl PA, Harrod C. 2013. Parallel and nonparallel ecological, morphological and genetic divergence in lake-stream stickleback from a single catchment. *J. Evol. Biol.* 26:186–204.

Reich D, Thangaraj K, Patterson N, Price AL, Singh L. 2009. Reconstructing Indian population history. *Nature* 461:489–494.

Richards TJ, Ortiz-Barrientos D. 2016. Immigrant inviability produces a strong barrier to gene flow between parapatric ecotypes of *Senecio lautus*. *Evolution* 70:1239–1248.

Richards TJ, Walter GM, McGuigan K, Ortiz-Barrientos D. 2016. Divergent natural selection drives the evolution of reproductive isolation in an Australian wildflower. *Evolution* 70:1993–2003.

Roda F, Ambrose L, Walter GM, Liu HL, Schaul A, Lowe A, Pelser PB, Prentis P, Rieseberg LH, Ortiz-Barrientos D. 2013. Genomic evidence for the parallel evolution of coastal forms in the *Senecio lautus* complex. *Mol. Ecol.* 22:2941–2952.

Roda F, Liu H, Wilkinson MJ, Walter GM, James ME, Bernal DM, Melo MC, Lowe A, Rieseberg LH, Prentis P, et al. 2013. Convergence and divergence during the

adaptation to similar environments by an Australian groundsel. *Evolution* 67:2515–2529.

Roesti M, Gavrilets S, Hendry AP, Salzburger W, Berner D. 2014. The genomic signature of parallel adaptation from shared genetic variation. *Mol. Ecol.* 23:3944–3956.

Roesti M, Kueng B, Moser D, Berner D. 2015. The genomics of ecological vicariance in threespine stickleback fish. *Nat. Commun.* 6:8767.

Rohland N, Reich D. 2012. Cost-effective, high-throughput DNA sequencing libraries for multiplexed target capture. *Genome Res.* 22:939–946.

Rosenblum EB, Parent CE, Brandt EE. 2014. The molecular basis of phenotypic convergence. *Annu. Rev. Ecol. Evol. Syst.* 45:203–226.

Rougemont Q, Gaigher A, Lasne E, Côte J, Coke M, Besnard AL, Launey S, Evanno G. 2015. Low reproductive isolation and highly variable levels of gene flow reveal limited progress towards speciation between European river and brook lampreys. *J. Evol. Biol.* 28:2248–2263.

Rougeux C, Bernatchez L, Gagnaire PA. 2017. Modeling the multiple facets of speciation-with-gene-flow toward Inferring the divergence history of lake whitefish species pairs (Coregonus clupeaformis). *Genome Biol. Evol.* 9:2057–2074.

Rougeux C, Gagnaire PA, Bernatchez L. 2019. Model-based demographic inference of introgression history in European whitefish species pairs'. *J. Evol. Biol.* 32:806–817.

Roux C, Fraïsse C, Romiguier J, Anciaux Y, Galtier N, Bierne N. 2016. Shedding light on the grey sone of speciation along a continuum of genomic divergence. *PLoS Biol* 14:e2000234.

Schluter D. 2000. The ecology of adaptive radiation. Oxford: Oxford University Press

Schluter D, Nagel LM. 1995. Parallel speciation by natural selection. *Am. Nat.* 146:292–301.

Schmieder R, Lim YW, Rohwer F, Edwards R. 2010. TagCleaner: Identification and removal of tag sequences from genomic and metagenomic datasets. *BMC Bioinform.* 11:341.

Schrempf D, Minh BQ, De Maio N, von Haeseler A, Kosiol C. 2016. Reversible polymorphism-aware phylogenetic models and their application to tree inference. *J. Theor. Biol.* 407:362–370.

Slatkin M. 1985a. Gene flow in natural populations. *Annu. Rev. Ecol. Syst.* 16:393–430.

Slatkin M. 1985b. Rare alleles as indicators of gene flow. *Evolution* 39:53–65.

Slatkin M. 1993. Isolation by distance in equilibrium and non-equilibrium populations. *Evolution* 47:264–279.

Smith SD, Rausher MD. 2011. Gene loss and parallel evolution contribute to species difference in flower color. *Mol. Biol. Evol.* 28:2799–2810.

Stern DL, Orgogozo V. 2009. Is genetic evolution predictable? *Science* 323:746–751.

Stoltzfus A, McCandlish DM. 2017. Mutational biases influence parallel adaptation. *Mol. Biol. Evol.* 34:2163–2172.

Storz JF, Wheat CW. 2010. Integrating evolutionary and functional approaches to infer adaptation at specific loci. *Evolution* 64:2489–2509.

Strasburg JL, Rieseberg LH. 2008. Molecular demographic history of the annual sunflowers *Helianthus annuus* and *H. petiolaris*-large effective population sizes and rates of long-term gene flow. *Evolution* 62:1936–1950.

Strasburg JL, Rieseberg LH. 2010. How robust are "Isolation with Migration" analyses to violations of the IM model? A simulation study. *Mol. Biol. Evol.* 27:297–310.

Tan A, Abecasis GR, Kang HM. 2015. Unified representation of genetic variants. *Bioinformatics* 31:2202–2204.

Thomé MTC, Carstens BC. 2016. Phylogeographic model selection leads to insight into the evolutionary history of four-eyed frogs. *PNAS* 113:8010–8017.

Thompson IR. 2005. Taxonomic studies of Australian *Senecio* (Asteraceae): 5. The *S. pinnatifolius/S. lautus* complex. *Muelleria* 21:23–76.

Tiffin P, Ross-Ibarra J. 2014. Advances and limits of using population genetics to understand local adaptation. *Trends Ecol. Evol.* 29:673–680.

Trucchi E, Frajman B, Haverkamp THA, Schönswetter P, Paun O. 2017. Genomic analyses suggest parallel ecological divergence in *Heliosperma pusillum* (Caryophyllaceae). *New Phytol.* 216:267–278.

Walter GM, Aguirre JD, Blows MW, Ortiz-Barrientos D. 2018. Evolution of genetic variance during adaptive radiation. *Am. Nat.* 191:E108–E128.

Walter GM, Wilkinson MJ, Aguirre JD, Blows MW, Ortiz-Barrientos D. 2018. Environmentally induced development costs underlie fitness tradeoffs. *Ecology* 99:1391–1401.

Walter GM, Wilkinson MJ, James ME, Richards TJ, Aguirre JD, Ortiz-Barrientos D. 2016. Diversification across a heterogeneous landscape. *Evolution* 70:1979–1992.

Wilkinson MJ, Roda F, Walter GM, James ME, Nipper R, Walsh J, North HL, Beveridge CA, Ortiz-Barrientos D. 2021. Adaptive divergence in shoot gravitropism creates hybrid sterility in an Australian wildflower. Preprint at https://doi.org/10.1101/845354.

Wolfram Research, Inc. 2020. Mathematica. Version 12.2. Champaign, Illinois. https://www.wolfram.com/mathematica

Wright S. 1943. Isolation by distance. *Genetics* 28:114–138.

Yeaman S. 2015. Local adaptation by alleles of small effect. *Am. Nat.* 186:S74–S89.

Yeaman S, Gerstein AC, Hodgins KA, Whitlock MC. 2018. Quantifying how constraints limit the diversity of viable routes to adaptation. *PLoS Genet.* 14:e1007717.

York RA, Fernald RD. 2017. The repeated evolution of behavior. *Front. Ecol. Evol.* 4:143.

Figures

Fig 1. The colonization history and phylogenetic topology for alternate origin scenarios

Schematic diagram representing the colonization history and phylogenetic topology of two ecotypes (dark green and light green) from an ancestral population (grey) for three origin scenarios. Solid arrows depict the sequence of colonization. Double headed dotted arrows represent gene flow (*m*) between the ecotypes within each locality. L1, L2 and L3 represent three geographically distant localities, where a population of each ecotype resides. **(A)** Within a single origin scenario, the two ecotypes arise once from the ancestor, followed by range expansion. In the absence of gene flow, ecotypes form monophyletic clades within the phylogeny. **(B)** The single origin with gene flow scenario involves gene flow upon secondary contact between the ecotypes within each locality. Here, the observed phylogenetic topology shows populations clustering according to their geographic distribution. **(C)** Within a multiple origin scenario, the ancestral (dark green) ecotype arises once from the ancestor followed by range expansion, with the derived (light green) populations independently arising from each dark green population. Populations phylogenetically cluster according to their geographic distribution, which can be indistinguishable from a single origin with gene flow scenario **(B)**.

Fig 2. Sampling locations and genetic clustering of *Senecio lautus* populations

(A) Sampling locations of the 23 Dune (orange) and Headland (green) *Senecio lautus* populations along the coast of Australia. **(B)** Maximum likelihood phylogeny of Dune and Headland populations implemented in *IQ-TREE*. Numbers on each node represent the SH-alRT support (%), followed by the ultrafast bootstrap support (%). **(C)** Bayesian assignment of individuals to genetic clusters within *fastSTRUCTURE* for K=2-4. Each of the 1,319 individuals is depicted as a bar, with colors representing ancestry proportions to each cluster. Populations are ordered according to their geographic distribution along the coast.

Fig 3. Patterns of long-distance gene flow, isolation by distance, and genetic clustering

(A) Maximum likelihood tree with one migration event inferred in *TreeMix*, the x-axis representing genetic drift. The red arrow represents the migration event (w = 0.40). **(B)** Patterns of isolation by distance using Slatkin's $\widehat{M}$ for parapatric Dune-Headland (black), Dune-Dune (orange) and Headland-Headland (green) pairs. Black dashed line represents the

linear model for the DH comparisons. **(B)** Patterns of isolation by distance across Dune and Headland populations for Dune-Headland (DH, black), Dune-Dune (DD, orange) and Headland-Headland (HH, green) pairs. Average migration rate is the mean bidirectional migration for each pair estimated in *fastsimcoal2*. Grey shading represents the null expectation for migration rates, inferred from the maximum migration value from three allopatric comparisons ($2Nm = 0.33$). Grey horizontal dashed line represents one migrant per generation ($2Nm = 1$). Pairs falling above this line are labelled. Black dashed line represents the linear model for the DH comparisons. **(D)** Bayesian assignment of individuals to genetic clusters within *fastSTRUCTURE* for K=23. Each of the 1,319 individuals is depicted as a bar, with colors representing ancestry proportions to each cluster. Populations are ordered according to their geographic distribution along the coast.

Fig 4. Patterns of gene flow and admixture between parapatric Dune-Headland populations

(A) Bayesian assignment of individuals to genetic clusters within *STRUCTURE* for K=2 for the Dune (dark green) and Headland (light green) ecotypes at each locality. Each individual is depicted as a bar, with colors representing ancestry proportions to each cluster. Below are the migration rates (m, forward in time) for the most likely divergence model for Dune to Headland, and Headland to Dune within each locality estimated within *fastsimcoal2*. Asterisks denote pairs with $2Nm > 1$. **(B)** Schematic diagram representing the ten demographic models run in *fastsimcoal2* and their estimated parameters: no migration (NM), bidirectional migration (BM), population 2 to population 1 migration (M21), population 1 to population 2 migration (M12), bidirectional migration after secondary contact (BSC), population 2 to population 1 migration after secondary contact (SC21), population 1 to population 2 migration after secondary contact (SC12), bidirectional migration after population splitting with cessation of gene flow (EBM), ancient bidirectional secondary contact (ASC), population size reduction after bidirectional secondary contact (PRSC).

Fig 5. Coalescent modelling to infer the probability of non-monophyly

(A) Schematic diagram representing the modelled single origin scenario. *t2* represents the time to the split of the ancestral population (i.e., the initial origin of the Dune and Headland ecotypes). Each of these two ecotypes further split at time *t1* in the past. Parapatric populations at each locality are connected with dashed lines, and an instantaneous burst of

migration (*m*) occurs at time *tm* in the past (dashed horizontal red line). In the model, all times are expressed in units of 2*N* generations. Light green and dark green circles represent populations from different ecotypes. **(B, C)** Probability of non-monophyly, falsely suggesting the parallel evolution of ecotypes. *tm* is set 0.1 (corresponding to 50,000 generations for a diploid population size of 250,000). Small phylogenies are schematic diagrams of the extreme values of the y-axis. **(B)** High probability of non-monophyly occurs when internal branches (IB) are short (lower yellow region). *t1* is set to 1 (corresponding to 500,000 generations for N=250,000). **(C)** The probability of non-monophyly requires high migration and increases when length of terminal branches (TB) are longer prior to the burst of migration (right-hand yellow region). *t2* is set to 1 (corresponding to 500,000 generations). Note the different scale of probability in panel **(C)** compared to panel **(B)**.

Fig 1.

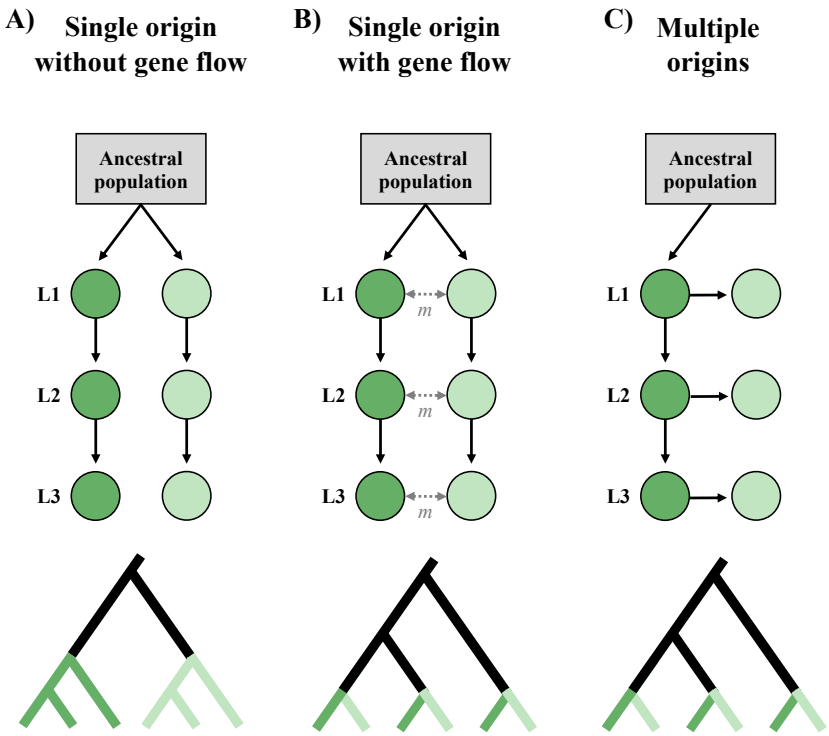
A)
Single origin without gene flow
B)
Single origin with gene flow
C)
Multiple origins
Ancestral population
Ancestral population
Ancestral population
L1
L2
L3
L1
L2
L3
m
m
m
L1
L2
L3

Fig 2.

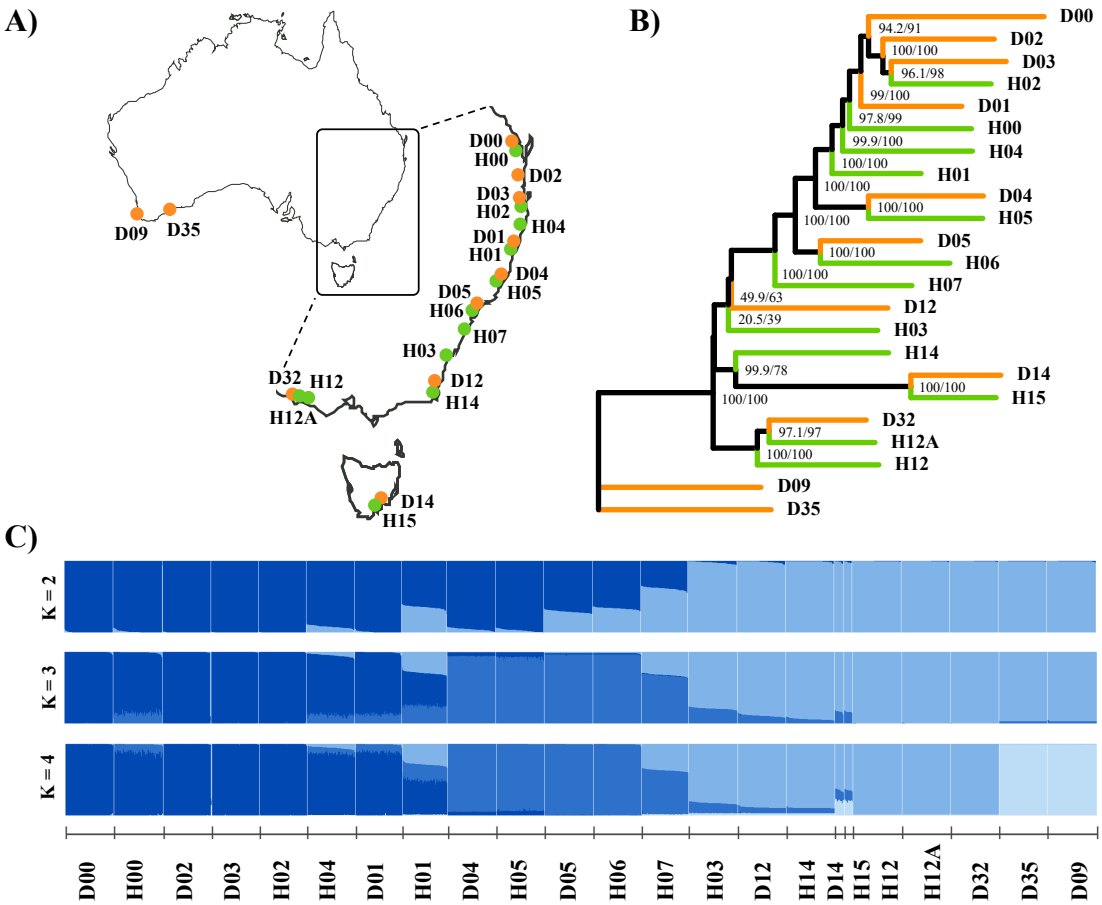
A)
D00
H00
D02
D03
H02
H04
D01
H01
D04
H05
D05
H06
H07
H03
D12
H14
D32
H12
H12A
D09
D35
D14
H15
B)
D00
94.2/91
D02
100/100
D03
96.1/98
H02
99/100
D01
97.8/99
H00
99.9/100
H04
100/100
H01
100/100
D04
100/100
H05
100/100
D05
100/100
H06
100/100
H07
49.9/63
D12
20.5/39
H03
H14
99.9/78
D14
100/100
H15
100/100
D32
97.1/97
H12A
100/100
H12
D09
D35
C)
K = 2
K = 3
K = 4
D00
H00
D02
D03
H02
H04
D01
H01
D04
H05
D05
H06
H07
H03
D12
H14
D14
H15
H12
H12A
D32
D35
D09

Fig 3.

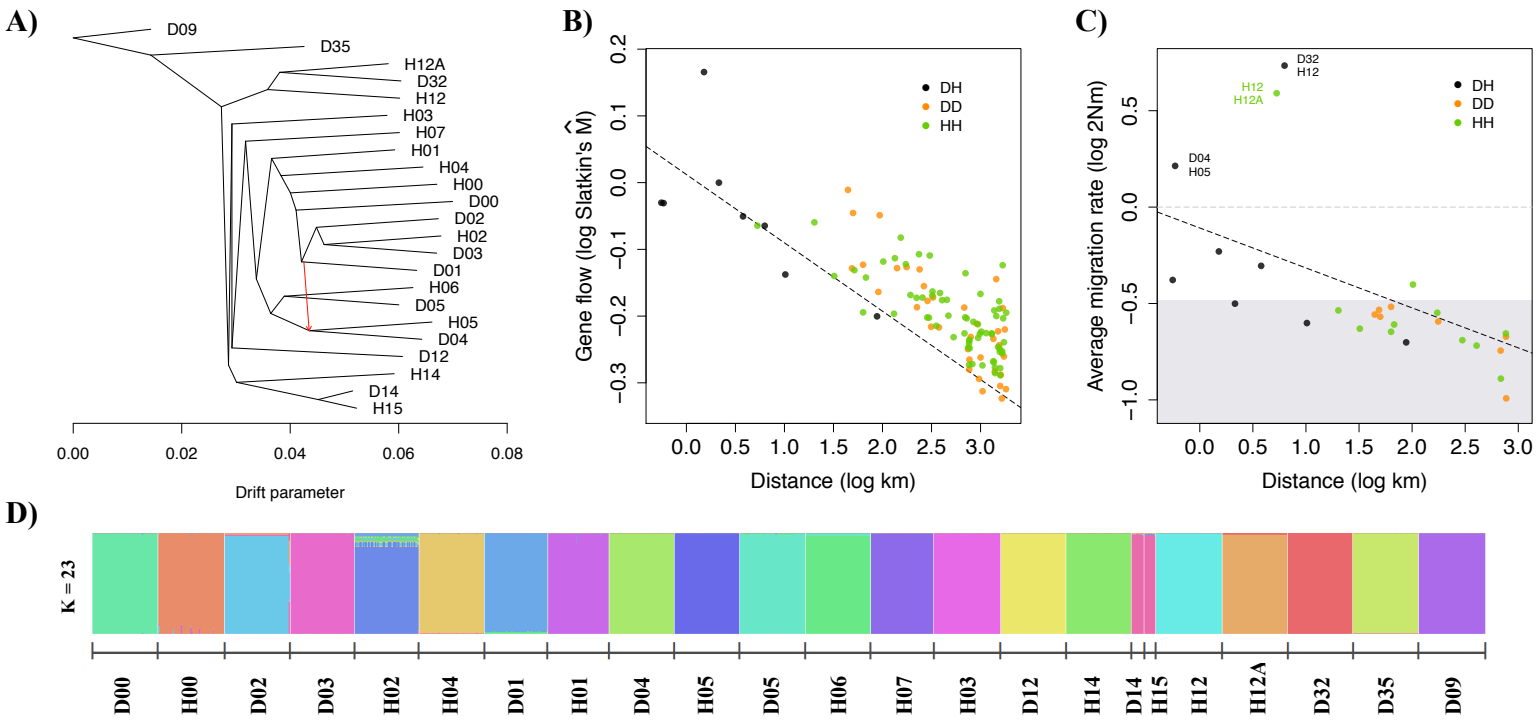
A)
D09
D35
H12A
D32
H12
H03
H07
H01
H04
H00
D00
D02
H02
D03
D01
H06
D05
H05
D04
D12
H14
D14
H15
0.00
0.02
0.04
0.06
0.08
Drift parameter
B)
Gene flow (log Slatkin's M̂)
Distance (log km)
DH
DD
HH
C)
Average migration rate (log 2Nm)
Distance (log km)
D32
H12
H12
H12A
D04
H05
DH
DD
HH
D)
K = 23
D00
H00
D02
D03
H02
H04
D01
H01
D04
H05
D05
H06
H07
H03
D12
H14
D14
H15
H12
H12A
D32
D35
D09

Fig 4.

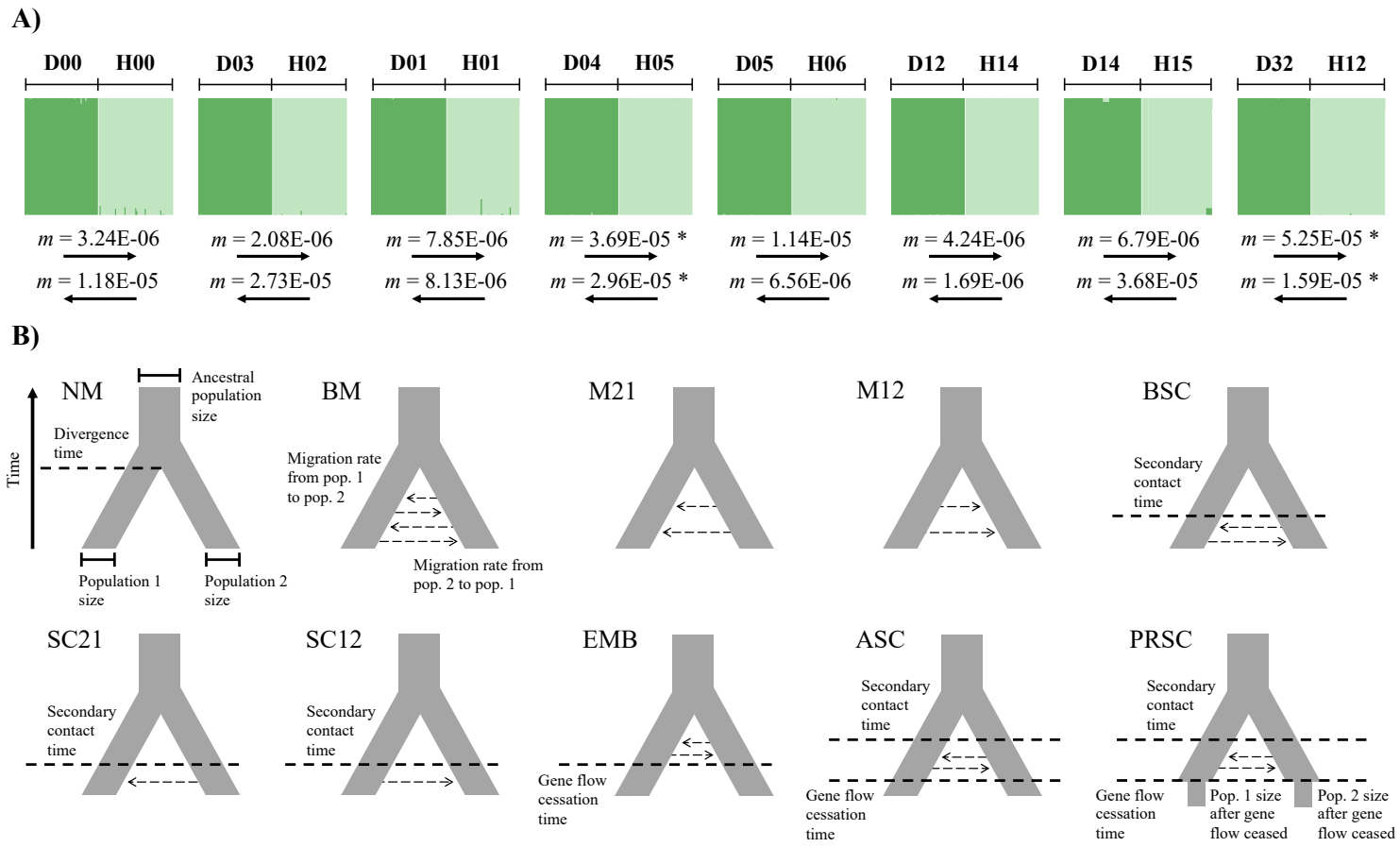
A)
D00
H00
D03
H02
D01
H01
D04
H05
D05
H06
D12
H14
D14
H15
D32
H12
m = 3.24E-06
m = 1.18E-05
m = 2.08E-06
m = 2.73E-05
m = 7.85E-06
m = 8.13E-06
m = 3.69E-05 *
m = 2.96E-05 *
m = 1.14E-05
m = 6.56E-06
m = 4.24E-06
m = 1.69E-06
m = 6.79E-06
m = 3.68E-05
m = 5.25E-05 *
m = 1.59E-05 *
B)
NM
Ancestral population size
Divergence time
Time
Population 1 size
Population 2 size
BM
Migration rate from pop. 1 to pop. 2
Migration rate from pop. 2 to pop. 1
M21
M12
BSC
Secondary contact time
SC21
Secondary contact time
SC12
Secondary contact time
EMB
Gene flow cessation time
ASC
Secondary contact time
Gene flow cessation time
PRSC
Secondary contact time
Gene flow cessation time
Pop. 1 size after gene flow ceased
Pop. 2 size after gene flow ceased

Fig 5.

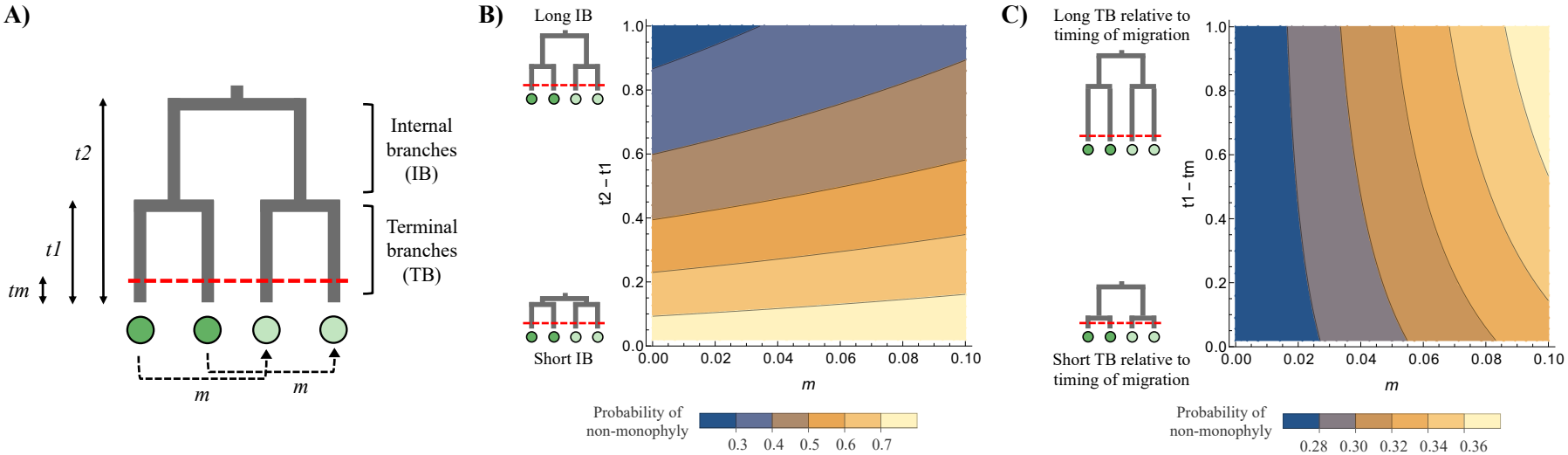
A)
t2
t1
tm
m
m
Internal branches (IB)
Terminal branches (TB)
B)
Long IB
Short IB
t2 – t1
m
Probability of non-monophyly
0.3 0.4 0.5 0.6 0.7
C)
Long TB relative to timing of migration
Short TB relative to timing of migration
t1 – tm
m
Probability of non-monophyly
0.28 0.30 0.32 0.34 0.36